

# Chiral Glass: A New Equilibrium Phase of Ceramic High- $T_c$ Superconductors

Hikaru Kawamura

*Faculty of Engineering and Design, Kyoto Institute of Technology,  
Sakyo-ku, Kyoto 606, Japan*

Mai Suan Li

*Institute of Physics, Polish Academy of Sciences, 02-668 Warsaw, Poland*

## Abstract

Possible occurrence of an equilibrium thermodynamic phase with a spontaneously broken time-reversal symmetry is studied in a model ceramic superconductor with anisotropic pairing symmetry. It is shown by Monte Carlo simulations that such a “chiral-glass” phase is truly stable even under the influence of screening. Existence of frustration in zero external field, arising from the  $d$ -wave pairing symmetry of high- $T_c$  superconductors, is essential to realize this phase. Via a finite-size scaling analysis, critical exponents associated with the chiral-glass transition are estimated to be  $\nu_{CG} = 1.3 \pm 0.2$  and  $\eta_{CG} = -0.2 \pm 0.2$ . These values turn out to be close to those of the Ising spin glass. Phase diagram of the model is constructed and the implications to experiments are discussed.

e-mail: kawamura@hie.kit.ac.jp

KEYWORDS: chiral glass, high- $T_c$  superconductors, Josephson junction, screening, frustration, chirality, nonlinear susceptibility, spin glass, vortex glass, Monte Carlo simulation, critical exponents.

# 1 Introduction

Among a variety of macroscopic thermodynamic properties of superconductors, the type and the nature of possible thermodynamic phases is of central importance. For example, considerable attention has recently been paid to the possible phase of high- $T_c$  superconductors in applied magnetic fields.<sup>1</sup> For sufficiently random or dirty samples, the existence of a true thermodynamic phase with zero linear resistance was predicted (a vortex-glass phase).<sup>2</sup> Recent numerical works suggest, however, that the screening effects eventually destabilize the vortex-glass phase.<sup>3</sup> In zero external field, by contrast, the only thermodynamic phase known to date either in clean or random superconductors is the standard Meissner phase.

Meanwhile, recent experimental studies have revealed that cuprate high- $T_c$  superconductors have an anisotropic pairing symmetry, probably of the  $d_{x^2-y^2}$ -wave type.<sup>4</sup> Naturally, one may expect that such anisotropic nature of the superconducting order parameter could give rise to novel thermodynamic properties not encountered in the conventional  $s$ -wave superconductors, possibly the appearance of a new thermodynamic phase. Unfortunately, this appears not to be the case in clean single crystals, although enhanced effects of thermal fluctuations give rise to a variety of interesting phenomena in high- $T_c$  superconductors. This is because the  $d_{x^2-y^2}$ -wave order parameter is characterized by a single phase variable of the condensate as in the conventional superconductors, and the resulting Ginzburg-Landau Hamiltonian, which is known to well describe various macroscopic properties of superconductors, has essentially the same form as in the conventional superconductors. By contrast, in *ceramic* or *granular* high- $T_c$  samples, the situation may well differ because ceramic samples can be regarded as a random Josephson network and the anisotropic superconducting order parameter largely modifies the properties of the Josephson junction.

One remarkable effect is the appearance of the ‘ $\pi$  junction’ characterized by

the *negative* Josephson coupling,  $J < 0$ , across which the order parameter changes the phase by  $\pi$ . One important consequence of such  $\pi$  junctions is the appearance of frustration even in zero external field.<sup>5</sup> Frustration is borne by the ‘odd ring’, a closed junction-loop having odd numbers of  $\pi$  junctions. On the basis of a single-loop model in which high- $T_c$  ceramics were regarded as an ensemble of noninteracting junction-loops, Sigrist and Rice<sup>6</sup> successfully explained the paramagnetic Meissner effect observed experimentally in certain high- $T_c$  ceramic samples.<sup>7,8</sup> Magnetic moments spontaneously induced at the odd rings give rise to a paramagnetic response observed experimentally.

It is also evident, however, that the paramagnetic Meissner effect itself is not directly related to a new thermodynamic phase, since an ensemble of noninteracting junction-loops is enough to cause the paramagnetic susceptibility,<sup>6,9</sup> just as an ensemble of free spins gives rise to the paramagnetic Curie law. In the present paper, we wish to address the question whether a new type of equilibrium phase closely related to the unconventional pairing symmetry of high- $T_c$  superconductors is ever possible in certain ceramic samples. Indeed, one of the present authors (H.K.) recently proposed that such a novel thermodynamic phase might be realized in zero external field in certain ceramic high- $T_c$  superconductors.<sup>10</sup> This state is characterized by a spontaneously broken time-reversal symmetry with keeping the  $U(1)$  gauge symmetry, and is called a ‘chiral-glass phase’.<sup>11</sup> The order parameter is then a ‘chirality’, which represents the direction of the local loop-supercurrent over grains. From a symmetry consideration, the nonlinear susceptibility was predicted to diverge with a negative sign at the associated chiral-glass transition point. Frustration effect, which arises due to the random distribution of  $\pi$  junctions with the negative Josephson coupling, is essential to realize this phase. Note that in this chiral-glass state, unlike in the vortex-glass (gauge-glass) state under external fields, the phase of the condensate is *not* ordered, even randomly, on sufficient long

length and time scales: The ordering occurs only in the loop-supercurrents, or in the *chiralities*.

There are several experimental results which appear to corroborate the existence of such a novel glassy zero-field phase in ceramic high- $T_c$  superconductors. Since the discovery of high- $T_c$  superconductors, it has been known that ceramic high- $T_c$  samples often exhibit a glassy behavior reminiscent of the spin glass.<sup>12–14</sup> More recently, Leylekian, Ocio and Hammann observed via the noise and ac susceptibility measurements that LSCO ceramic samples showed a glassy behavior reminiscent of the spin glass *even in zero external field*.<sup>15</sup> They also observed an intergranular cooperative phenomenon indicative of a glassy phase transition. It appears natural to interpret this cooperative phenomenon in terms of the proposed chiral-glass picture. More direct support of the chiral glass has recently been reported by the ac susceptibility measurements on YBCO ceramic samples. Thus, Matsuura *et al* observed a negatively divergent nonlinear susceptibility at an intergranular transition point,<sup>16</sup> consistent with the proposed chiral-glass picture.

It should be emphasized here, however, that the theoretical analysis of Ref.10 was based on an analogy to the  $XY$  spin glass,<sup>17</sup> and completely neglected the effects of screening (coupling of the condensate to fluctuating magnetic fields). Thus, the fate of the proposed chiral-glass phase in the presence of screening is not yet clear. It should be noted that the screening effect could be substantial in the intergranular ordering of ceramic high- $T_c$  materials, since the length unit to be compared with the penetration depth is the grain size ( $\sim 1\mu m$ ) rather than the short coherence length of the Cooper pair. As the screening effect makes the otherwise long-ranged interaction between the chirality (quenched-in half a vortex) short-ranged, one may wonder if it would eventually wash out a sharp phase transition and destabilize the chiral glass phase, just as it destabilizes the vortex-glass phase of type-II superconductors in a field.

The purpose of the present paper is to investigate the stability of the hypothetical chiral-glass phase against this screening effect, and to determine whether the chiral-glass state really exists as a true thermodynamic phase or not. For this purpose, we perform extensive Monte Carlo simulations on a frustrated three-dimensional lattice model introduced by Domínguez *et al.*,<sup>18</sup> in which the phase variables located at each site of the lattice are coupled to the fluctuating magnetic-field variables at each link. The model can also be viewed as a spin-glass-type (*i.e.*, random and frustrated) version of a  $U(1)$  lattice gauge theory. The same model was studied previously by Monte Carlo simulations with an interest in the behavior of linear<sup>18</sup> and nonlinear<sup>19</sup> susceptibilities. But, neither of these previous simulations was fully equilibrated, and thus, could not give any information whether a true equilibrium phase could exist or not. In the present paper, we perform equilibrium simulations on the same model based on an extended ensemble method recently proposed by Hukushima and Nemoto,<sup>20</sup> trying to determine the equilibrium properties of the model. A part of the results was already reported in Ref.21.

The remainder of this paper is organized as follows. In §2, we introduce our model and several physical quantities of interest. In §3, we give technical details of our Monte Carlo simulation. The results of Monte Carlo simulation are presented and analyzed in §4. By studying the Binder ratio associated with the chirality, we show that there indeed exists a stable chiral-glass phase with a spontaneously broken time-reversal symmetry even in the presence of screening. Critical exponents characterizing the chiral-glass transition are determined with use of a finite-size scaling analysis. Phase diagram of the model is also constructed. Section 5 is devoted to summary and discussion. We discuss in some detail the implications of the obtained results to the possible experimental detection of the chiral-glass state in ceramic high- $T_c$  superconductors. In particular, requirements for the appropriate samples as well as the method of detection are examined.

## 2 Model

We assume that weak links connecting the neighboring grains are distributed sufficiently dense, so that the system can be viewed as an infinite network of Josephson junctions which are not decomposed into finite clusters. Putting superconducting grains at the sites of a simple-cubic lattice, we model such ceramic superconductors by a three-dimensional lattice model of Josephson-junction array with finite self-inductance. Neglecting the charging effects of the grain, we consider the following zero-field Hamiltonian,<sup>18,19</sup>

$$\mathcal{H} = - \sum_{\langle ij \rangle} J_{ij} \cos(\theta_i - \theta_j - A_{ij}) + \frac{1}{2\mathcal{L}} \left( \frac{\phi_0}{2\pi} \right)^2 \sum_p (\vec{\nabla} \times \vec{A})^2, \quad (2.1)$$

where  $\theta_i$  is the phase of the condensate of the grain at the  $i$ -th site of a simple cubic lattice,  $\vec{A}$  being the fluctuating gauge potential at each link of the lattice,  $\phi_0$  the flux quantum,  $J_{ij}$  the Josephson coupling between the  $i$ -th and  $j$ -th grains, and the lattice curl  $\vec{\nabla} \times \vec{A}$  is the directed sum of  $A_{ij}$ 's round a plaquette.  $\mathcal{L}$  is the self-inductance of a loop (an elementary plaquette), while the mutual inductance between different loops is neglected. The first sum is taken over all nearest-neighbor pairs, while the second sum is taken over all elementary plaquettes on the lattice. Fluctuating thermodynamic variables to be summed over are the phase variables,  $\theta_i$ , at each site and the gauge variables,  $A_{ij}$ , at each link.

In this model, quenched randomness occurs only in the distribution of the Josephson coupling,  $J_{ij}$ , which is assumed to be an independent random variable taking the values  $J$  or  $-J$  with equal probability ( $\pm J$  or binary distribution), each representing  $0$  and  $\pi$  junctions. We also assume that  $J_{ij}$  is independent of temperature and magnetic field. This assumption is more or less justified when the intergranular ordering occurs at a temperature considerably lower than the

superconducting transition temperature of the grain. While our simulation is performed for this particular distribution of  $J_{ij}$ , one could expect from experience in spin-glass studies that the results would be rather insensitive to the details of the distribution, *e.g.*, a slight asymmetry between  $\pm J$  or the detailed form of the distribution.

The bare Josephson penetration depth in units of lattice spacing is given by

$$\lambda_0 = 1/\sqrt{\tilde{\mathcal{L}}}, \quad (2.2)$$

where  $\tilde{\mathcal{L}}$  is the dimensionless inductance defined by

$$\tilde{\mathcal{L}} = (2\pi/\phi_0)^2 J\mathcal{L}. \quad (2.3)$$

Thus, larger inductance corresponds to smaller penetration depth with enhanced effects of screening. In the limit  $\tilde{\mathcal{L}} \rightarrow 0$ , or  $\lambda_0 \rightarrow \infty$ , the screening effect becomes negligible and one recovers the  $XY$  spin-glass Hamiltonian of Ref.10. In the opposite limit  $\tilde{\mathcal{L}} \rightarrow \infty$ , on the other hand, it can be shown that the model reduces to the noninteracting one.<sup>19</sup> Therefore, the system remains in the disordered state even at  $T = 0$  in this limit.

The symmetry property of the Hamiltonian (2.1) was analyzed in detail in Ref.19. Contrary to the vortex-glass (gauge-glass) Hamiltonian, the Hamiltonian (2.1), defined in zero field, keeps the  $Z_2$  time-reversal symmetry in addition to the  $U(1)$  gauge symmetry. Frustration arises from the random distribution of both positive and negative Josephson couplings. This should be contrasted to the vortex-glass (gauge-glass) problem, where the associated Hamiltonian does not possess the time-reversal symmetry due to external magnetic fields, while the frustration arises from the magnetic field, not from the  $J_{ij}$ .

The Hamiltonian (2.1) can also be written in the dimensionless form as

$$\tilde{\mathcal{H}} \equiv \frac{\mathcal{H}}{J} = - \sum_{\langle ij \rangle} \tilde{J}_{ij} \cos(\theta_i - \theta_j - A_{ij}) + \frac{1}{2\tilde{\mathcal{L}}} \sum_p (\vec{\nabla} \times \vec{A})^2, \quad (2.4)$$

where  $\tilde{J}_{ij} \equiv J_{ij}/J$  is the dimensionless quenched random variable, taking values  $\pm 1$  with equal probability.

The local chirality may be defined at each plaquette by the gauge-invariant quantity,<sup>19</sup>

$$\kappa_p = 2^{-3/2} \sum_{\langle ij \rangle}^p \tilde{J}_{ij} \sin(\theta_i - \theta_j - A_{ij}), \quad (2.5)$$

where the sum runs over a directed contour along the sides of the plaquette  $p$ . Physically, the chirality,  $\kappa_p$ , is a half ( $\pi$ ) vortex, being proportional to the loop-supercurrent circulating round a plaquette  $p$ . If the plaquette  $p$  is frustrated, the local chirality  $\kappa_p$  tends to take a finite value, its sign representing either clockwise or counterclockwise orientation of circulating supercurrent. If, on the other hand, the plaquette is unfrustrated, it tends to take a value around zero. Note that the chirality is a pseudoscalar in the sense that it is invariant under global  $U(1)$  gauge transformation,  $\theta_i \rightarrow \theta_i + \Delta\theta$ ,  $A_{ij} \rightarrow A_{ij}$ , but changes its sign under global  $Z_2$  time-reversal transformation,  $\theta_i \rightarrow -\theta_i$ ,  $A_{ij} \rightarrow -A_{ij}$ . Due to this symmetry property, chirality can be regarded as an order parameter of the chiral order.

Induced local flux or magnetization threading a plaquette  $p$  is given in the dimensionless form by,

$$f_p = \frac{\Phi_p}{\phi_0}, \quad \Phi_p = \vec{\nabla} \times \vec{A}. \quad (2.6)$$

Flux is also a pseudoscalar like chirality, whose sign represents the direction of the induced magnetic moment threading the plaquette  $p$ . Total magnetization per plaquette along the  $z$ -axis is given by

$$m = \frac{1}{4\pi S N_p} \sum_{p \in \langle xy \rangle} \Phi_p, \quad (2.7)$$

where  $S$  is the area of a plaquette and the sum is taken over all  $N_p$  plaquettes on the  $\langle xy \rangle$  plane of the lattice. The corresponding dimensionless quantity,  $\tilde{m}$ , can

be defined by

$$\tilde{m} \equiv \frac{4\pi S}{\phi_0} m = \frac{1}{N_p} \sum_{p \in \langle xy \rangle} f_p. \quad (2.8)$$

The linear susceptibility,  $\chi$ , is given by<sup>18,19</sup>

$$\chi \equiv \frac{dm}{dH} = \frac{\pi \tilde{\beta} N_p}{\tilde{\mathcal{L}}} [\langle \tilde{m}^2 \rangle] - \frac{1}{4\pi}, \quad (2.9)$$

where  $H$  is an external magnetic field,  $\tilde{\beta}$  is the dimensionless inverse temperature defined by  $\tilde{\beta} = J/k_B T$ ,  $\langle \dots \rangle$  represents a thermal average, and  $[\dots]$  represents a configurational average over the bond distribution. The linear susceptibility is dimensionless in cgs units. The nonlinear susceptibility,  $\chi_2$ , or its dimensionless counterpart,  $\tilde{\chi}_2$ , is given by<sup>19</sup>

$$\begin{aligned} \chi_2 &= \frac{1}{6} \frac{d^3 m}{dH^3} \equiv \left( \frac{4\pi S}{\phi_0} \right)^2 \tilde{\chi}_2, \\ \tilde{\chi}_2 &= \frac{1}{6} \left( \frac{\pi \tilde{\beta} N_p}{\tilde{\mathcal{L}}} \right)^3 [\langle \tilde{m}^4 \rangle - 3 \langle \tilde{m}^2 \rangle^2]. \end{aligned} \quad (2.10)$$

In these expressions of  $\chi$  and  $\chi_2$ , we omit the parts which are odd under the time-reversal operation,  $m \rightarrow -m$ : In zero external field, such odd parts should vanish identically in any finite system in full equilibrium. Note that the above  $\chi_2$ , being proportional to the minus of the third-harmonic component of the ac susceptibility, is sometimes denoted as  $\chi_3$  in the literature.

### 3 Monte Carlo simulation

We perform Monte Carlo simulations for the Hamiltonian (2.1) based on the standard Metropolis method combined with an extended ensemble method. Several values of the dimensionless inductance,  $\tilde{\mathcal{L}}$ , are simulated including  $\tilde{\mathcal{L}} = 1, 3, 4, 5$ , with the greatest effort in the case of  $\tilde{\mathcal{L}} = 1$ . Since the bare penetration depth,  $\lambda_0$ , in those cases is equal to, or less than one lattice spacing, we expect that the effect

of screening should manifest itself even for rather small lattices studied here, which contain  $L \times L \times L$  sites with  $L = 3, 4, 6, 8, 10$ . Sample average is taken over 1540 ( $L = 3$ ), 1000 ( $L = 4$ ), 500 ( $L = 6$ ), 300 ( $L = 8$ ) and 100 ( $L = 10$ ) independent bond realizations.

We impose free boundary conditions on all sides of the lattice. If, on the other hand, one applies the standard periodic boundary conditions on the link variables  $A_{ij}$ 's, one has somewhat unphysical results that the magnetization vanishes trivially even under external fields. In zero field, the periodic boundary conditions imposed on the link variables  $A_{ij}$ 's also lead to the trivial vanishing of the susceptibility. In view of such unphysical nature of the periodic boundary conditions, we impose free boundary conditions in the following simulations.

Monte Carlo simulation is performed according to the version of an extended ensemble method of Ref.20, where the whole configurations at two neighboring temperatures of the same sample are occasionally exchanged. In this method, one simulates the sample with a given bond realization at  $N_T$  distinct temperatures at a time distributed in the range  $[T_{min}, T_{max}]$ . Monte Carlo updating consists of the two parts: The first part is the standard local Metropolis updating at each temperature, and the second part is an exchange of the whole lattices at two neighboring temperatures.

Since the present spin-glass-like model possesses the link variable,  $A_{ij}$ , in addition to the site variable,  $\theta_i$ , an equilibrium simulation is rather hard even with the new efficient algorithm. In the case of  $L = 8$ , for example, we prepare 20 temperature points distributed in the range  $[0.27\text{J}, 0.8\text{J}]$  for a given sample, and perform  $1.5 \times 10^5$  exchanges per temperature of the whole lattices combined with the same number of standard 'single-spin-flip' Metropolis sweeps.<sup>20</sup> Equilibration is checked by monitoring the stability of the results against at least three-times longer runs for a subset of samples.

As long as one is interested in the gauge-invariant quantities like the chirality or the flux, the results would not depend on the particular choice of the gauge. In most of our calculation, we choose the gauge where the  $A_{ij}$ 's along the  $z$ -direction are fixed to be zero. We also use other gauges to take some limited data, including the Coulomb gauge and the 'temporal gauge',<sup>18,19</sup> just to make sure that the results are really independent of the choice of the gauge.

We run in parallel two independent replicas with the same bond realization and compute an overlap between the chiral variables in the two replicas,<sup>17</sup>

$$q_\kappa = \frac{1}{N_p} \sum_p \kappa_p^{(1)} \kappa_p^{(2)}. \quad (3.1)$$

In terms of this chiral overlap,  $q_\kappa$ , the Binder ratio of the chirality is calculated by

$$g_{\text{CG}} = \frac{1}{2} \left( 3 - \frac{[\langle q_\kappa^4 \rangle]}{[\langle q_\kappa^2 \rangle]^2} \right). \quad (3.2)$$

Here  $g_{\text{CG}}$  is normalized so that in the thermodynamic limit it tends to zero above the chiral-glass transition temperature,  $T_{\text{CG}}$ , and tends to unity below  $T_{\text{CG}}$  provided the ground state is non-degenerate. At the chiral-glass transition point, curves of  $g_{\text{CG}}$  against  $T$  for different  $L$  should intersect asymptotically.

The chiral-glass susceptibility, which is expected to diverge at the chiral-glass transition point, is given by

$$\chi_{\text{CG}} = N_p [\langle q_\kappa^2 \rangle], \quad (3.3)$$

The behavior of the chiral short-range order may be seen via the mean magnitude of the local chirality,  $\bar{\kappa}$ , defined by

$$\bar{\kappa} = \left\{ \frac{1}{N_p} \sum_p [\langle \kappa_p^2 \rangle] \right\}^{1/2}. \quad (3.4)$$

Note that for the frustrated noncollinear configurations,  $\bar{\kappa}$ , tends to take a finite value whereas for the unfrustrated collinear configurations  $\bar{\kappa}$  tends to vanish. One

can also define a reduced chiral-glass susceptibility,  $\tilde{\chi}_{\text{CG}}$ , corrected for the short-range order effect by dividing  $\chi_{\text{CG}}$  by the appropriate power of the magnitude of the local chirality,<sup>17</sup>

$$\tilde{\chi}_{\text{CG}} = \chi_{\text{CG}}/\bar{\kappa}^4. \quad (3.5)$$

Similarly to the case of the chirality, one can introduce an overlap between the flux variables in the two independent replicas,

$$q_f = \frac{1}{N_p} \sum_p f_p^{(1)} f_p^{(2)}. \quad (3.6)$$

In terms of  $q_f$ , the Binder ratio of the flux is calculated by

$$g_{\text{FG}} = \frac{1}{2} \left( 3 - \frac{[\langle q_f^4 \rangle]}{[\langle q_f^2 \rangle]^2} \right). \quad (3.7)$$

The flux-glass susceptibility,  $\chi_{\text{FG}}$ , and its reduced counterpart,  $\tilde{\chi}_{\text{FG}}$ , are defined by

$$\chi_{\text{FG}} = N_p [\langle q_f^2 \rangle], \quad (3.8)$$

$$\tilde{\chi}_{\text{FG}} = \chi_{\text{FG}}/\bar{f}^4, \quad (3.9)$$

respectively, where the the mean magnitude of the local flux is defined by

$$\bar{f} = \left\{ \frac{1}{N_p} \sum_p [\langle f_p^2 \rangle] \right\}^{1/2}. \quad (3.10)$$

## 4 Monte Carlo results

In this section, we present the results of our Monte Carlo simulations. Most extensive simulation is made for the inductance  $\tilde{\mathcal{L}} = 1$ , which corresponds to the bare penetration depth,  $\lambda_0$ , equal to one lattice spacing. In the subsection [A], we present our Monte Carlo results for this inductance,  $\tilde{\mathcal{L}} = 1$ . The results for other inductances including  $\tilde{\mathcal{L}} = 3, 4, 5$  will be presented later in the subsection [B].

[A]  $\tilde{\mathcal{L}} = 1$

In Fig.1, the temperature dependence of the root-mean square of the local-chirality amplitude,  $\bar{\kappa}$ , defined by Eq.(3.4), is shown for various lattice sizes. Even at lower temperatures  $\bar{\kappa}$  keeps a nonzero value, slightly increasing with decreasing temperature, which indicates that the chiral short-range order is developed in the temperature range studied here.

Fig.2a displays the size and temperature dependence of the Binder ratio of the chirality,  $g_{CG}$ . The data of  $g_{CG}$  for  $L = 3, 4, 6, 8$  all cross at almost the same temperature  $T \sim 0.28-0.29$ , strongly suggesting the occurrence of a finite-temperature chiral-glass transition at  $T_{CG} = 0.286 \pm 0.01$  (temperature  $T$  is measured in units of  $J$ ). In particular, the data below  $T_{CG}$  show a rather clear fan out.

The determined value of  $T_{CG}$  is slightly lower than the corresponding chiral-glass transition temperature of the pure  $\pm J$   $XY$  spin glass determined in Ref.17,  $T_{CG} = 0.32 \pm 0.01$ . Note that the spin-glass model corresponds to the  $\tilde{\mathcal{L}} \rightarrow 0$  limit of the present model. The observed suppression of  $T_{CG}$  by the screening effect seems reasonable, since the screening effect makes the long-ranged interaction between vortices (chiralities) short-ranged, which should make the chiral-glass transition less favorable.

The value of the Binder ratio at the transition point,  $g_{CG}^*$ , is estimated to be  $g_{CG}^* \simeq 0.38$ . The estimated value is considerably smaller than the corresponding value of the 3D  $XY$  spin glass,<sup>17</sup>  $g_{CG}^* \simeq 0.72$ . This large deviation probably comes from the difference in the choice of boundary conditions, *i.e.*, free boundary conditions in the present simulation and periodic boundary conditions in Ref.17. Note that the value of  $g^*$  is known to depend on the choice of boundary conditions even in a given universality class.

Standard finite-size scaling analysis is made for  $g_{CG}$  based on the one-parameter

fit of the form,

$$g_{\text{CG}} = \bar{g}_{\text{CG}}(L^{1/\nu_{\text{CG}}} | T - T_{\text{CG}} |), \quad (4.1)$$

with fixing  $T_{\text{CG}} = 0.286$ , where  $\bar{g}_{\text{CG}}$  is a scaling function. Then, the chiral correlation-length exponent  $\nu_{\text{CG}}$  is estimated to be  $\nu_{\text{CG}} = 1.3 \pm 0.2$ . The corresponding finite-size-scaling plot is given in Fig.2b.

The temperature and size dependence of the reduced chiral-glass susceptibility,  $\tilde{\chi}_{\text{CG}}$ , defined by eq.(3.5), are shown in Fig.3a. Finite-size scaling analysis based on the relation,

$$\tilde{\chi}_{\text{CG}} = L^{2-\eta_{\text{CG}}} \bar{\tilde{\chi}}_{\text{CG}}(L^{1/\nu_{\text{CG}}} | T - T_{\text{CG}} |), \quad (4.2)$$

is made with fixing  $T_{\text{CG}} = 0.286$  and  $\nu_{\text{CG}} = 1.3$ , yielding the chiral critical-point-decay exponent  $\eta_{\text{CG}} = -0.2 \pm 0.2$ . The resulting finite-size-scaling plot is displayed in Fig.3b. Other exponents can be estimated via the standard scaling relations as  $\gamma_{\text{CG}} \simeq 2.9$  and  $\beta_{\text{CG}} \simeq 0.5$ .

The obtained chiral-glass exponents are rather close to the values determined previously for the  $\pm J$  XY spin glass, *i.e.*, the model without screening;  $\nu_{\text{CG}} = 1.5 \pm 0.3$  and  $\eta_{\text{CG}} = -0.4 \pm 0.2$ .<sup>17</sup> Therefore, our present result seems consistent with the view that the screening effect is actually irrelevant at the 3D chiral-glass transition.

It should be noted here that the determined chiral-glass exponents are also not far from the standard spin-glass exponents of the 3D Ising spin glass.<sup>22,23</sup> In recent Monte Carlo simulations of the 3D Ising spin glass, however, considerably different values were reported for the exponent  $\nu$ , depending on whether  $\nu$  was determined from the scaling of the Binder ratio,  $g$ , or from the scaling of the spin-glass susceptibility,  $\chi_{\text{SG}}$ . In Ref.22, for example, the former procedure gave an estimate  $\nu \simeq 2.0$  while the latter procedure gave  $\nu \simeq 1.6$ , whereas in Ref.23, the former gave  $\nu \simeq 3.0$  and the latter gave  $\nu \simeq 1.5$ . By contrast, in the present

simulation, we did not observe such significant discrepancy between the estimated values of  $\nu_{\text{CG}}$ : A common value of  $\nu_{\text{CG}} \simeq 1.3$  gave satisfactory fits both for  $g_{\text{CG}}$  and  $\tilde{\chi}_{\text{CG}}$ . At present, we are not sure whether such apparent difference from the standard Ising spin glass is simply due to finite-size effects, or is suggesting the possibility that the universality class of the chiral-glass transition and that of the Ising spin glass are in fact different. Since the chirality can be viewed as a “continuous” Ising variable, there exists an obvious similarity between the chiral glass and the pure Ising spin glass from a symmetry viewpoint. By contrast, in the present model, there exists a local constraint on the possible configurations of the chiral variables,<sup>24</sup> which is absent in the Ising spin glass. This may possibly change the universality class of the transition. Further studies are required to clarify this point.

Anyway, the occurrence of an equilibrium ordered phase appears to be clear from our numerical data, and is in sharp contrast to the vortex-glass (gauge-glass) problem where the screening was found to destabilize the equilibrium ordered phase.<sup>3</sup> Presumably, such difference comes from the fact that the broken symmetry is a discrete  $Z_2$  symmetry here while it is a continuous  $U(1)$  symmetry in Ref.3.

We also study the behavior of the flux. The temperature dependence of the root-mean square of the local-flux amplitude,  $\bar{f}$ , defined by Eq.(3.10), is shown in Fig.4. As can be seen from the figure, the magnitude of the induced local flux is of order 0.1 flux quantum per plaquette for this inductance ( $\tilde{\mathcal{L}} = 1$ ). Note that, in the small inductance limit  $\tilde{\mathcal{L}} \rightarrow 0$ ,  $\bar{f}$  tends to zero, while in the large inductance limit  $\tilde{\mathcal{L}} \rightarrow \infty$ ,  $\bar{f}$  tends to 1/2 in the ground state of an isolated *frustrated* plaquette.

The flux Binder ratio,  $g_{\text{FG}}$ , defined by Eq.(3.7), and the reduced flux-glass susceptibility,  $\tilde{\chi}_{\text{FG}}$ , defined by Eq.(3.9), are shown in Fig.5, and 6, respectively. Naively, one expects that the flux should behave in the same way as the chirality, since the flux is also a pseudoscalar variable sharing the same symmetry as the

chirality. Indeed, as can be seen from Fig.6, the flux-glass susceptibility,  $\tilde{\chi}_{\text{FG}}$ , shows a divergent behavior similar to  $\tilde{\chi}_{\text{CG}}$ . However, in contrast to the naive expectation, clear crossing of the Binder ratio as observed in  $g_{\text{CG}}$  is not observed in  $g_{\text{FG}}$  at least in the range of lattice sizes studied here: see Fig.5. Rather, the ordering tendency seems more enhanced in the sense that  $g_{\text{FG}}$  tends to increase with increasing  $L$  exhibiting a feature of the ordered phase even above  $T_{\text{CG}} \simeq 0.286$ . As the flux is an *induced* quantity generated by the finite inductance effect, we believe this behavior to be a finite-size effect. Presumably, for this inductance value, the flux hardly reaches its asymptotic critical behavior in rather small lattices studied here. Recall that, in the  $\tilde{\mathcal{L}} \rightarrow 0$  limit, the flux vanishes trivially while the chiral-glass transition itself is most favored. In fact, for larger inductances, we have found that the Binder ratios of the flux and of the chirality show more similar behavior as expected (see below).

We also compute the zero-field linear and nonlinear susceptibilities,  $\chi$  and  $\chi_2$ , defined by Eqs.(2.9) and (2.10), respectively. As can be seen from Fig.7, the linear susceptibility turns out to be paramagnetic,  $\chi > 0$ , over an entire temperature range studied, including in the disordered phase  $T > T_{\text{CG}}$ , without a clear anomaly at  $T_{\text{CG}}$ . In shorter simulations on the same model where the full equilibration is not achieved,  $\chi$  tends to get smaller and sometimes becomes negative.<sup>19</sup> These results seem consistent with an earlier finding of Domínguez *et al* who observed a paramagnetic  $\chi$  in the field-cooling mode, but a diamagnetic  $\chi$  in the zero-field-cooling mode.<sup>18</sup> Meanwhile, the simulation of Ref.18 was performed for a rather large inductance,  $\tilde{\mathcal{L}} = 8$ , where the chiral-glass transition probably did not occur in equilibrium (see below). It should be stressed here that the sign of  $\chi$  is in fact a nonuniversal property: Effects not taken into the present model, such as the contribution of intragranular supercurrents, could give additional diamagnetic contribution in real systems and could easily change the sign of the observed  $\chi$ .

By contrast, on general theoretical grounds, the nonlinear susceptibility,  $\chi_2$ , is expected to show a negative divergence at the transition point where the time-reversal symmetry is spontaneously broken in a spatially random manner.<sup>10</sup> Indeed, as shown in Fig.8(a), we have observed a behavior fully consistent with this expectation. The exponent associated with this negative divergence is estimated via a finite-size scaling analysis with assuming  $T_{CG} = 0.286$  and  $\nu_{CG}=1.3$ , yielding  $\gamma_2 \simeq 4.4$  (see Fig.8b), where  $\chi_2 \sim |T - T_{CG}|^{-\gamma_2}$ . This value of  $\gamma_2$  is somewhat larger than the chiral-glass susceptibility exponent,  $\gamma_{CG} \simeq 2.9$ . At present, it is not entirely clear whether this deviation reflects a true difference in the asymptotic critical behavior. It appears likely that the observed larger value of  $\gamma_2$  simply comes from a finite-size effect related to the possible nonasymptotic behavior of the flux as observed in  $g_{FG}$ .

[B]  $\tilde{\mathcal{L}} = 3, 4$  and 5

So far, the results reported were exclusively for the inductance  $\tilde{\mathcal{L}} = 1$ . We have also made similar, but less extensive simulations for other inductances  $\tilde{\mathcal{L}} = 3, 4, 5$  in order to study the inductance dependence of the chiral-glass ordering.

In Figs.9 and 10, the temperature and inductance dependence of the magnitude of the local chirality,  $\bar{\kappa}$ , and that of the local flux,  $\bar{f}$ , are shown for a fixed lattice size  $L = 6$ . With increasing  $\tilde{\mathcal{L}}$ ,  $\bar{\kappa}$  tends to be suppressed while  $\bar{f}$  tends to be enhanced. In Fig.11(a)-(c), the temperature dependence of the chiral Binder ratio,  $g_{CG}$ , is shown for  $\tilde{\mathcal{L}} = 3, 4$  and 5, respectively. For  $\tilde{\mathcal{L}} = 3, 4$ , the curves of  $g_{CG}$  for different  $L$  appear to cross at a finite temperature. As expected, the chiral-glass transition temperature monotonically decreases as  $\tilde{\mathcal{L}}$  increases. For  $\tilde{\mathcal{L}} = 5$ , on the other hand, no crossing of  $g_{CG}$  is observed in the temperature range  $T \geq 0.1$ , suggesting that the chiral-glass transition is highly suppressed at this inductance. We have also tried similar simulations for even larger inductances,  $\tilde{\mathcal{L}} > 5$ . However, the relaxation becomes extremely slow for these larger inductances, and we can no

longer equilibrate the system down to the temperature range of interest within a reasonable amount of computation time.

The tendency that the chiral-glass ordering is suppressed at larger inductances can also be seen from other quantities, such as the reduced chiral-glass susceptibility,  $\tilde{\chi}_{\text{CG}}$ , the reduced flux-glass susceptibility,  $\tilde{\chi}_{\text{FG}}$ , and the nonlinear susceptibility,  $\tilde{\chi}_2$ . Thus, we show in Fig.12, 13 and 14 the temperature and inductance dependence of  $\tilde{\chi}_{\text{CG}}$ ,  $\tilde{\chi}_{\text{FG}}$  and  $\tilde{\chi}_2$  for a fixed lattice size  $L = 6$ . As can clearly be seen in these figures, the chiral-glass ordering is more and more suppressed for larger  $\tilde{\mathcal{L}}$ . By contrast, the paramagnetic tendency of the linear susceptibility tends to be enhanced for larger  $\tilde{\mathcal{L}}$ . This is evident from Fig.15 in which the temperature and inductance dependence of the linear susceptibility,  $\chi$ , is shown for a fixed lattice size  $L = 6$ .

The obtained phase diagram in the  $T - \tilde{\mathcal{L}}$  plane is sketched in Fig.16. There appears to be a finite critical value of the inductance,  $\tilde{\mathcal{L}}_c$ , above which there is no equilibrium chiral-glass transition. Although it is difficult to precisely locate  $\tilde{\mathcal{L}}_c$  due to the extremely slow relaxations we observed at lower temperatures, it appears to lie around  $5 \lesssim \tilde{\mathcal{L}}_c \lesssim 7$ . If this is the case, the value of the inductance chosen by Domínguez *et al*<sup>18</sup> lied in the region of the phase diagram where no equilibrium chiral-glass transition took place. Then, a kind of cooperative phenomenon accompanied with a sharp growth of the paramagnetic  $\chi$ , which was observed around  $T \simeq 0.4$  in Ref.18, might not be related to an equilibrium phase transition, but be purely of dynamical origin. This is consistent with our observation in Fig.15 that the paramagnetic tendency is more enhanced for larger  $\tilde{\mathcal{L}}$ , while the chiral-glass ordering itself is suppressed for larger  $\tilde{\mathcal{L}}$ .

In Figs.17(a) and (b), we show the temperature dependence of the flux Binder ratio,  $g_{\text{FG}}$ , for the case of  $\tilde{\mathcal{L}} = 4$  and 5, respectively. In the case of  $\tilde{\mathcal{L}} = 4$ , the curves of  $g_{\text{FG}}$  of  $L = 4$  and  $L = 6$  almost cross, while they do not cross for  $\tilde{\mathcal{L}} = 5$ . Such

behavior is more or less similar to the one observed in the corresponding chiral Binder ratio,  $g_{CG}$ , for these inductances: see Figs.11(b) and (c). This observation suggests that for these larger inductances the flux behaves in the same way as the chirality even in rather small lattices studied here, in contrast to the  $\tilde{\mathcal{L}} = 1$  case.

## 5 Summary and discussion

We have shown by extensive Monte Carlo simulations that an equilibrium zero-field phase with a spontaneous broken time-reversal symmetry, a chiral-glass phase, is possible in certain ceramic superconductors with anisotropic pairing symmetry. This phase is truly stable even in the presence of screening. As in spin glasses, the nonlinear susceptibility exhibits a negative divergence at the chiral-glass transition point. Via a finite-size scaling, static exponents associated with the chiral-glass transition are determined. The obtained exponents are rather close to those of the 3D Ising spin glass. A rough phase diagram is constructed in the temperature-inductance plane. It is found that the chiral-glass transition tends to be suppressed for larger inductances, and there appears to be a critical value of the parameter  $\tilde{\mathcal{L}}$  beyond which there is no equilibrium chiral-glass phase. By contrast, the paramagnetic tendency of the linear susceptibility (paramagnetic Meissner effect) tends to be enhanced for larger inductances. This observation clearly shows that, although the paramagnetic Meissner effect could also arise from the frustration effect associated with the anisotropic nature of the superconducting order parameter, it has no direct relevance to the chiral-glass phase and the chiral-glass transition.

Next, on the basis of our findings in the present paper, we wish to discuss some requirements for the appropriate ceramic samples where one could expect the chiral-glass phase. One important parameter characterizing the sample is the dimensionless inductance,  $\tilde{\mathcal{L}}$ , given by Eq.(2.3). Our present result suggests that an

equilibrium chiral-glass state could be realized in the type of samples with smaller  $\tilde{\mathcal{L}}$ , but not for the samples with larger  $\tilde{\mathcal{L}}$ . If one models a loop as a cylinder of radius  $r$  and height  $h$ , its inductance is given by  $\mathcal{L} = 4\pi^2 r^2/h$ . Putting  $r \sim 1\mu\text{m}$ ,  $h/r \sim 0.01$  and  $J \sim 20\text{K}$  (these values are chosen to mimic the sample used in Ref.16), one gets  $\tilde{\mathcal{L}} \sim 10^{-2}$ . Since this value is considerably smaller than  $\tilde{\mathcal{L}}_c$ , an equilibrium chiral-glass phase may well occur in such samples. By contrast, if the sample has too large a grain size or too strong Josephson coupling, an equilibrium chiral-glass phase will not be realized, or at least largely suppressed. Another requirement for the sample is that the grains must be connected via weak links into an infinite cluster, not decomposed into finite clusters. Obviously, finite-cluster samples cannot exhibit a chiral-glass transition, although the paramagnetic Meissner effect is still possible.<sup>6,9</sup>

Once appropriate samples could be prepared, the chiral-glass transition is detectable in principle via the standard magnetic measurements by looking for a negative divergence of  $\chi_2$  or a magnetic ageing phenomenon, as in the case of spin glasses. In such magnetic measurements, care has to be taken to keep the intensity of applied ac and dc fields weak enough, typically much less than 1G, so that the external flux per loop is sufficiently smaller than  $\phi_0$ . Recently, a sharp negatively-divergent anomaly of  $\chi_2$  was reported in a  $\text{YB}_2\text{C}_4\text{O}_8$  ceramic sample by the ac method by Matsuura *et al.*,<sup>16</sup> which might be a signal of the chiral-glass transition. Ageing was observed in certain ceramic samples,<sup>25</sup> but not in other samples.<sup>9</sup>

As in the case of spin glasses, measurements of dynamic susceptibilities such as  $\chi'(\omega)$  and  $\chi''(\omega)$  would also give useful information on the possible chiral-glass ordering, particularly when combined with the dynamic scaling analysis. For example, near the chiral-glass transition point, the imaginary part of the linear susceptibility,  $\chi''(\omega)$ , is expected to satisfy the dynamic scaling relation of the form,

$$\chi''(\omega, T, H) \approx \omega^{\beta_{\text{CG}}/z_{\text{CG}}\nu_{\text{CG}}} \bar{\chi}''\left(\frac{\omega}{t^{z_{\text{CG}}\nu_{\text{CG}}}}, \frac{H^2}{t^{\beta_{\text{CG}}+\gamma_{\text{CG}}}}\right), \quad (5.1)$$

where  $t \equiv |(T - T_{\text{CG}})/T_{\text{CG}}|$  and  $z_{\text{CG}}$  is a dynamical chiral-glass exponent. From the present calculation, we get the static chiral-glass exponents to be  $\nu_{\text{CG}} \simeq 1.3$ ,  $\beta_{\text{CG}} \simeq 0.5$  and  $\beta_{\text{CG}} + \gamma_{\text{CG}} \simeq 3.4$ . Although we cannot give a direct numerical estimate of the dynamical exponent from the present simulation, one might guess that  $z_{\text{CG}}$  would take a value around  $z_{\text{CG}}\nu_{\text{CG}} \simeq 7 - 8$  if one would assume the analogy between the chiral glass and the Ising spin glass also in the dynamics.<sup>26</sup>

Indeed, a dynamic scaling analysis was made by Leylekian, Ocio and Hammann for LSCO ceramic samples.<sup>15</sup> These authors performed both the ac susceptibility and the noise measurements, and found an intergranular cooperative transition even in zero field at a temperature about 10% below the superconducting transition temperature of the grain. Note that the noise measurements enable one to probe truly zero-field phenomena where one can be free from the extrinsic pinning effects such as the ones envisaged in the so-called critical-state model.<sup>27</sup> It was then found that the data of  $\chi''$  satisfied the dynamic scaling of the form (5.1). Here note that one is *not* allowed to invoke the standard vortex-glass scenario to explain such intergranular cooperative transition *in zero field*, since in the standard vortex-glass picture frustration is possible only under finite external fields. By contrast, the experiment seems consistent with the chiral-glass picture.

Meanwhile, when the intragranular superconducting transition and the intergranular transition take place at mutually close temperatures as in Ref.15, the Josephson coupling,  $J$ , which has been assumed to be temperature independent in the present model, is actually strongly temperature dependent in the transition region. In such a case, care has to be taken in analyzing the experimental data, since such temperature dependence of  $J$  might modify the apparent exponent value from the true asymptotic value to some *effective value*. In fact, the dynamical exponent  $z\nu \simeq 30$  determined by Leylekian *et al* were different from the standard spin-glass value, which might be due to the proximity effect of the intragranular

superconducting transition.<sup>15</sup> If, on the other hand, the temperature dependence of  $J$  was taken into account in the fit, a more realistic value  $z\nu \simeq 10 - 15$  was obtained in Ref.15. By contrast, when the intergranular chiral-glass transition takes place at a temperature much lower than the intragranular superconducting transition temperature as in Ref.16, the Josephson coupling can safely be regarded as temperature independent as assumed in the present model. Anyway, it is desirable to get a direct numerical estimate of the dynamical chiral-glass exponent,  $z_{CG}$ , to be compared with experiments. We are now planning to perform a simulation to get an independent numerical estimate the dynamical exponent.

It may also be possible to detect a spontaneously induced flux in the chiral-glass state by muon spin relaxation or electron holography in zero external field. As in the noise measurements, these measurements can be made in zero external field, and has an advantage of being free from the pinning effects of extrinsic origin. Here it is essential to make such measurements for *ceramic* samples with sufficiently many weak links, not for single crystals, simply because the chiral-glass phase is expected only in the former type of samples. By contrast, the kind of time-reversal-symmetry breaking proposed by Wen, Wilczek and Zee is associated with the time-reversal-symmetry of the *bulk* superconducting order parameter and should occur *even in single crystals*.<sup>28</sup>

We could estimate an order of the induced flux below  $T_{CG}$  from the results of our present simulation. In the case of  $\tilde{\mathcal{L}} = 1$ , for example, the flux intensity can be estimated from the calculated  $[< q_f^2 >]$  to be about  $0.02\phi_0$  at 20% below  $T_{CG}$ . For a sample with a typical grain diameter about  $1\mu m$ , this corresponds to the flux intensity equal to 0.4G, which seems well within the sensitivity of the  $\mu SR$  measurements. For a sample with a grain diameter about  $10\mu m$ , the flux intensity would be reduced to 4mG. If the dimensionless inductance,  $\tilde{\mathcal{L}}$ , is significantly smaller than unity, the flux intensity would become much smaller, and eventually

vanishes in the  $\tilde{\mathcal{L}} \rightarrow 0$  limit.

In the chiral-glass state, the  $U(1)$  gauge symmetry will *not* be broken, even randomly, in the strict sense. This means that the phase of the condensate,  $\theta$ , remains disordered in the chiral-glass state at least on sufficiently long length and time scales. Thus, the chiral-glass state should not be a true superconductor, with a small but nonvanishing linear resistance even below  $T_{\text{CG}}$ . This property has been established in the  $\tilde{\mathcal{L}} \rightarrow 0$  limit where the screening effect can be neglected.<sup>10,17</sup> Although we have not measured in the present simulation the quantity directly relevant to the  $U(1)$  gauge-symmetry breaking, the screening effect makes the interaction between vortices short-ranged and makes the the  $U(1)$  gauge-symmetry breaking transition even more unlikely.

Small but finite linear resistivity,  $\rho_L$ , in the chiral-glass state arises due to the slow motion of thermally-activated *integer* vortex lines (unbound vortex loops). Free motion of integer vortex lines is still possible in the chiral-glass state where chiralities (half-vortices) sitting at frustrated plaquettes are frozen. A schematic picture showing such free motion of integer vortex-line excitations in the background of a frozen pattern of chiralities is given in Fig.18. One can see that free motion of integer-vortex lines of either sign is possible without seriously destroying the freezing pattern of chiralities in the background. In order to destroy the chiral-glass ordering in the background, a chiral domain-wall-type excitation is necessary, which would be responsible for the chiral-glass transition at  $T = T_{\text{CG}}$ . On decreasing the temperature across  $T_{\text{CG}}$ , a sharp drop of the resistivity will be caused by such chiral domain-wall excitations, but the resistivity will stay finite even below  $T_{\text{CG}}$  due to the wandering vortex-line excitations.

We try to get a very rough order estimate of  $\rho_L$  at the chiral-glass transition point based on a flux-creep model.<sup>29</sup> Within this model, the linear  $I - V$  relation with finite  $\rho_L$  is expected below a characteristic current-density scale,  $j_c$ , given by

$j_c \simeq k_B T / (\phi_0 d^2 \tilde{\xi}^2)$ , where  $d$  is a typical grain size and  $\tilde{\xi}$  is the phase correlation length (or the ‘spin’ correlation length) in units of  $d$ . We estimate  $\tilde{\xi}$  at  $T = T_{CG}$  from the Monte Carlo data of the 3D  $XY$  spin glass<sup>30,17</sup> to be  $\tilde{\xi} \sim 10$  lattice spacings. Here note that the spin-glass correlation length does not diverge at the chiral-glass transition point.<sup>17</sup> Then, for a typical ceramic sample, we put  $d \simeq 1\mu m$ ,  $T = T_{CG} \simeq 30K$ , to get  $j_c \simeq 2 \times 10^3 A/m^2$ . The flux-creep model also yields  $\rho_L \sim \phi_0^2 d \tilde{\xi} / (k_B T \tau_0 \tilde{\tau})$ , where  $\tau_0$  is an inverse ‘attempt frequency’ of the intergranular vortex motion, and  $\tilde{\tau}$  is the phase or ‘spin’ correlation time in units of  $\tau_0$ . Again, from the Monte Carlo data,<sup>30,17</sup> we estimate  $\tilde{\tau}$  at  $T = T_{CG}$  to be  $\tilde{\tau} \simeq 5 \times 10^4$  Monte Carlo time steps. Precise value of our time unit,  $\tau_0$ , is largely unknown, but it should be much longer than the atomic time scale since the vortex motion of interest here is the one over grains. If we put  $\tau_0 \simeq 10^{-9}$  sec, for example, we have  $\rho_L \simeq 0.2\mu\Omega\cdot cm$  at  $T = T_{CG}$ , while for  $\tau_0 \simeq 10^{-5}$  sec, we have  $\rho_L \simeq 0.2 \times 10^{-4}\mu\Omega\cdot cm$ . These values, though small, may be within the reach of careful experimental measurements.

All simulations presented in this paper were done in zero external field. A chiral-glass phase and a chiral-glass transition are associated with a spontaneously breaking of time-reversal symmetry, and in that sense, can be regarded as a zero-field phenomenon. Still, it should be emphasized here that the fate of the chiral-glass phase and the chiral-glass transition in an external field is not necessarily trivial and is of great interest. Clearly, under external magnetic fields, the system no longer possesses a global time-reversal symmetry. Therefore, there cannot be a chiral-glass transition associated with a spontaneous breaking of a *global* time-reversal symmetry. Nevertheless, an interesting possibility emerges if the chiral-glass transition in zero field accompanies the replica symmetry breaking<sup>31</sup> of the chirality. In such a case, an equilibrium phase and the associated thermodynamic transition should persist even under finite fields and are characterized by the *chiral*

*replica symmetry breaking*. Then, the transition line in the  $H - T$  plane might look like the so-called AT-line familiar in spin glasses.<sup>32</sup> It is very interesting to relate such *chiral*-AT line to the AT-like line often observed experimentally in ceramic high- $T_c$  superconductors.<sup>12</sup>

We finally note that the chiral-glass state can be realized not only in high- $T_c$  superconductors, but also in other superconductors with nontrivial pairing symmetry, such as in heavy fermion superconductors, or possibly, in some organic superconductors. It would be interesting to experimentally search for this novel phase in these materials, since it is a new state of matter realized only in anisotropic superconductors with unconventional pairing symmetry.

The numerical calculation was performed on the FACOM VPP500 at the supercomputer center, Institute of Solid State Physics, University of Tokyo. A part of this work was made when one of the authors (M.S. Li) was in Kyoto Institute of Technology. M.S. Li thanks the Japan Society for Promotion of Science for the award of a fellowship. He was also supported in part by the Polish KBN grant.

## References

- 1 G. Blatter, M.V. Feigel'man, V.B. Geshkenbein, A.I. Larkin and V.M. Vinokur, Rev. Mod. Phys. **66** (1994) 1125.
- 2 M.P.A. Fisher, Phys. Rev. Lett. **62** (1989) 1415.
- 3 H.S. Bokil and A.P. Young, Phys. Rev. Lett. **74**, (1995) 3021; C. Wengel and A.P. Young, Phys. Rev. **B54** (1996) R6869.
- 4 See, for example, A. Mathai, Y. Gim, R.C. Black, A. Amar and F.C. Wellstood, Phys. Rev. Lett. **74** (1995) 4523; D.J. van Harlingen, Rev. Mod. Phys. **67**, 515 (1995).
- 5 F.V. Kusmartsev, Phys. Rev. Lett. **69** (1992) 2268; J. of Superconductivity **5** (1992) 463.
- 6 M. Sigrist and T.M. Rice, J. Phys. Soc. Jpn. **61** (1992) 4283; Rev. Mod. Phys. **67** (1995) 503.
- 7 P. Svedlindh, K. Niskanen, P. Nordblad, L. Lundgren, B. Lönnberg and T. Lundström, Physica **C162-164** (1989) 1365.
- 8 W. Braunisch, N. Knauf, G. Bauer, A. Kock, A. Becker, B. Freitag, A. Grütz, V. Kataev, S. Neuhausen, B. Roden, D. Khomskii, D. Wohlleben, J. Bock and E. Preisler, Phys. Rev. **B48** (1993) 4030.
- 9 J. Magnusson, J.-O. Andersson, M. Björnander, P. Nordblad and P. Svedlindh, Phys. Rev. **B51** (1995) 12776; J. Magnusson, M. Björnander, L. Pust, P. Svedlindh, P. Nordblad and T. Lundström, Phys. Rev. **B52** (1995) 7675.
- 10 H. Kawamura, J. Phys. Soc. Jpn. **64** (1995) 711.

- 11 Note that the same state was also called ‘orbital-glass phase’ in Ref.10. Since the term ‘orbital-glass’ has often been used in the literature simply to describe the state exhibiting the paramagnetic Meissner effect, however, we do not use this terminology here to represent the thermodynamic phase of our interest, but rather, use the term ‘chiral-glass’, following the  $XY$  spin-glass terminology. In the chiral-glass phase, the susceptibility could be either paramagnetic or diamagnetic.
- 12 K.A. Müller, M. Takashige and J.G. Bednorz, Phys. Rev. Lett. **58** (1987) 1143.
- 13 Z. Koziol, Physica **C159** (1989) 281.
- 14 K. Park, J.J. Kim and J.C. Park, Solid State Comm. **71** (1989) 743.
- 15 L. Leylejian, M. Ocio and J. Hammann, Physica **C185-189** (1991) 2243; Physica **B194-196** (1994) 1865.
- 16 M. Matsuura, M. Kawachi, K. Miyoshi, M. Hagiwara and K. Koyama, J. Phys. Soc. Jpn. **64** (1995) 4540.
- 17 H. Kawamura, Phys. Rev. **B51** (1995) 12398; J. Phys. Soc. Jpn. **61** (1992) 3062; H. Kawamura and M. Tanemura, J. Phys. Soc. Jpn. **60** (1991) 608.
- 18 D. Domínguez, E.A. Jagla and C.A. Balseiro, Phys. Rev. Lett. **72** (1994) 2773.
- 19 H. Kawamura and M.S. Li, Phys. Rev. **B53** (1996) 619.
- 20 K. Hukushima and K. Nemoto, J. Phys. Soc. Jpn. **65** (1996) 1604.
- 21 H. Kawamura and M.S. Li, to appear in Phys. Rev. Lett. (1997).

- 22 N. Kawashima and A.P. Young, Phys. Rev. **B53** (1996) 484; A.P. Young and N. Kawashima, Int. J. Mod. Phys. **C7** (1996) 327.
- 23 K. Hukushima, H. Takayama and K. Nemoto, Int. J. Mod. Phys. **C7** (1996) 337.
- 24 J. Villain, J. Phys. **C11** (1978) 745.
- 25 C. Rossel, Y. Maeno and I. Morgenstern, Phys. Rev. Lett. **62** (1989) 681.
- 26 A.T. Ogielsky, Phys. Rev. **B32** (1985) 7384.
- 27 C.P. Bean, Rev. Mod. Phys. **36** (1964) 31.
- 28 X.G. Wen, F. Wilczek and A. Zee, Phys. Rev. **B39** (1989) 11413.
- 29 P.W. Anderson and Y.B. Kim, Rev. Mod. Phys. **36** (1964) 39.
- 30 S. Jain and A.P. Young: J. Phys. **C19** (1986) 3913.
- 31 G. Parisi, J. Phys. **A13** (1980) 1101.
- 32 J.R.L. de Almeida and D.J. Thouless, J. Phys. **A11** (1978) 983.

## Figure captions

- Fig. 1 The temperature and size dependence of the root-mean square of the local-chirality amplitude,  $\bar{\kappa}$ , defined by Eq.(3.4), for  $\tilde{\mathcal{L}} = 1$ .
- Fig. 2 (a) The temperature and size dependence of the Binder ratio of the chirality,  $g_{\text{CG}}$ , for  $\tilde{\mathcal{L}} = 1$ . Inset is a magnified view around the transition temperature  $T_{\text{CG}} \simeq 0.286$ . (b) Finite-size scaling plot of  $g_{\text{CG}}$  with  $T_{\text{CG}} = 0.286$  and  $\nu_{\text{CG}} = 1.3$ .
- Fig. 3 (a) The temperature and size dependence of the reduced chiral-glass susceptibility,  $\tilde{\chi}_{\text{CG}}$ , for  $\tilde{\mathcal{L}} = 1$ . (b) Finite-size scaling plot of  $\tilde{\chi}_{\text{CG}}$  with  $T_{\text{CG}} = 0.286$ ,  $\nu_{\text{CG}} = 1.3$  and  $\eta_{\text{CG}} = -0.2$ .
- Fig. 4 The temperature and size dependence of the root-mean square of the local-flux amplitude,  $\bar{f}$ , defined by Eq.(3.10), for  $\tilde{\mathcal{L}} = 1$ .
- Fig. 5 The temperature and size dependence of the Binder ratio of the flux,  $g_{\text{FG}}$ , for  $\tilde{\mathcal{L}} = 1$ .
- Fig. 6 The temperature and size dependence of the reduced flux-glass susceptibility,  $\tilde{\chi}_{\text{FG}}$ , for  $\tilde{\mathcal{L}} = 1$ .
- Fig. 7 The temperature and size dependence of the zero-field linear susceptibility,  $\chi$ , for  $\tilde{\mathcal{L}} = 1$ . An arrow in the figure represents the location of the chiral-glass transition point.
- Fig. 8 (a) The temperature and size dependence of the zero-field nonlinear susceptibility,  $\tilde{\chi}_2$ , for  $\tilde{\mathcal{L}} = 1$ . (b) Finite-size scaling plot of  $\tilde{\chi}_2$  with  $T_{\text{CG}} = 0.286$ ,  $\nu_{\text{CG}} = 1.3$  and  $\gamma_2 = 4.4$ , where  $\tilde{\chi}_2 \sim (T - T_{\text{CG}})^{-\gamma_2}$ . An arrow in the figure represents the location of the chiral-glass transition point.

Fig. 9 The temperature and inductance dependence of the root-mean square of the local-chirality amplitude,  $\bar{\kappa}$ , defined by Eq.(3.4), for a fixed lattice size  $L = 6$ .

Fig. 10 The temperature and inductance dependence of the root-mean square of the local-flux amplitude,  $\bar{f}$ , defined by Eq.(3.10), for a fixed lattice size  $L = 6$ .

Fig. 11 The temperature and size dependence of the Binder ratio of the chirality,  $g_{CG}$ , for (a)  $\tilde{\mathcal{L}} = 3$ , (b)  $\tilde{\mathcal{L}} = 4$  and (c)  $\tilde{\mathcal{L}} = 5$ .

Fig. 12 The temperature and inductance dependence of the reduced chiral-glass susceptibility,  $\tilde{\chi}_{CG}$ , for a fixed lattice size  $L = 6$ .

Fig. 13 The temperature and inductance dependence of the reduced flux-glass susceptibility,  $\tilde{\chi}_{FG}$ , for a fixed lattice size  $L = 6$ .

Fig. 14 The temperature and inductance dependence of the zero-field nonlinear susceptibility,  $\tilde{\chi}_2$ , for a fixed lattice size  $L = 6$ .

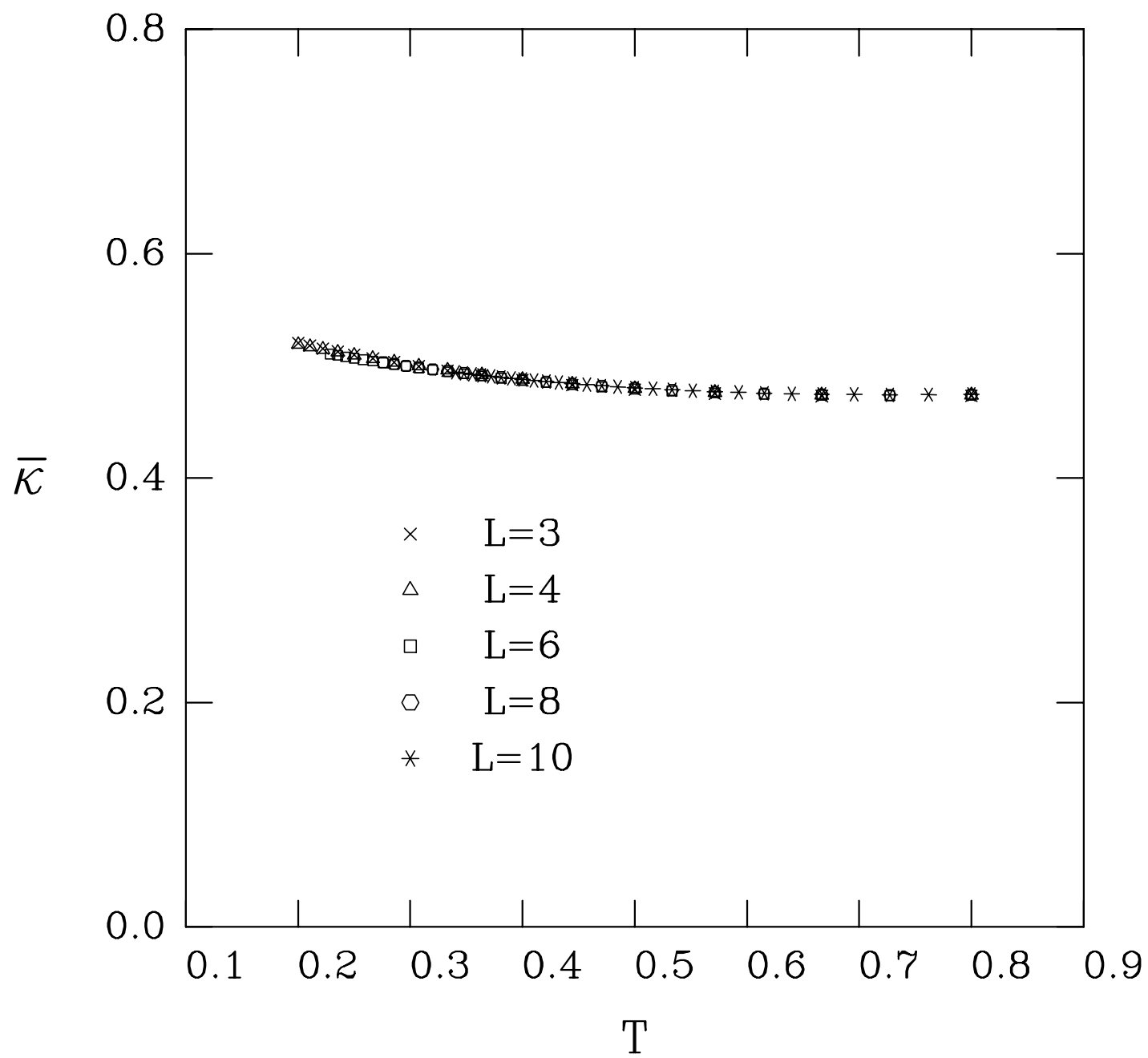
Fig. 15 The temperature and inductance dependence of the zero-field linear susceptibility,  $\chi$ , for a fixed lattice size  $L = 6$ .

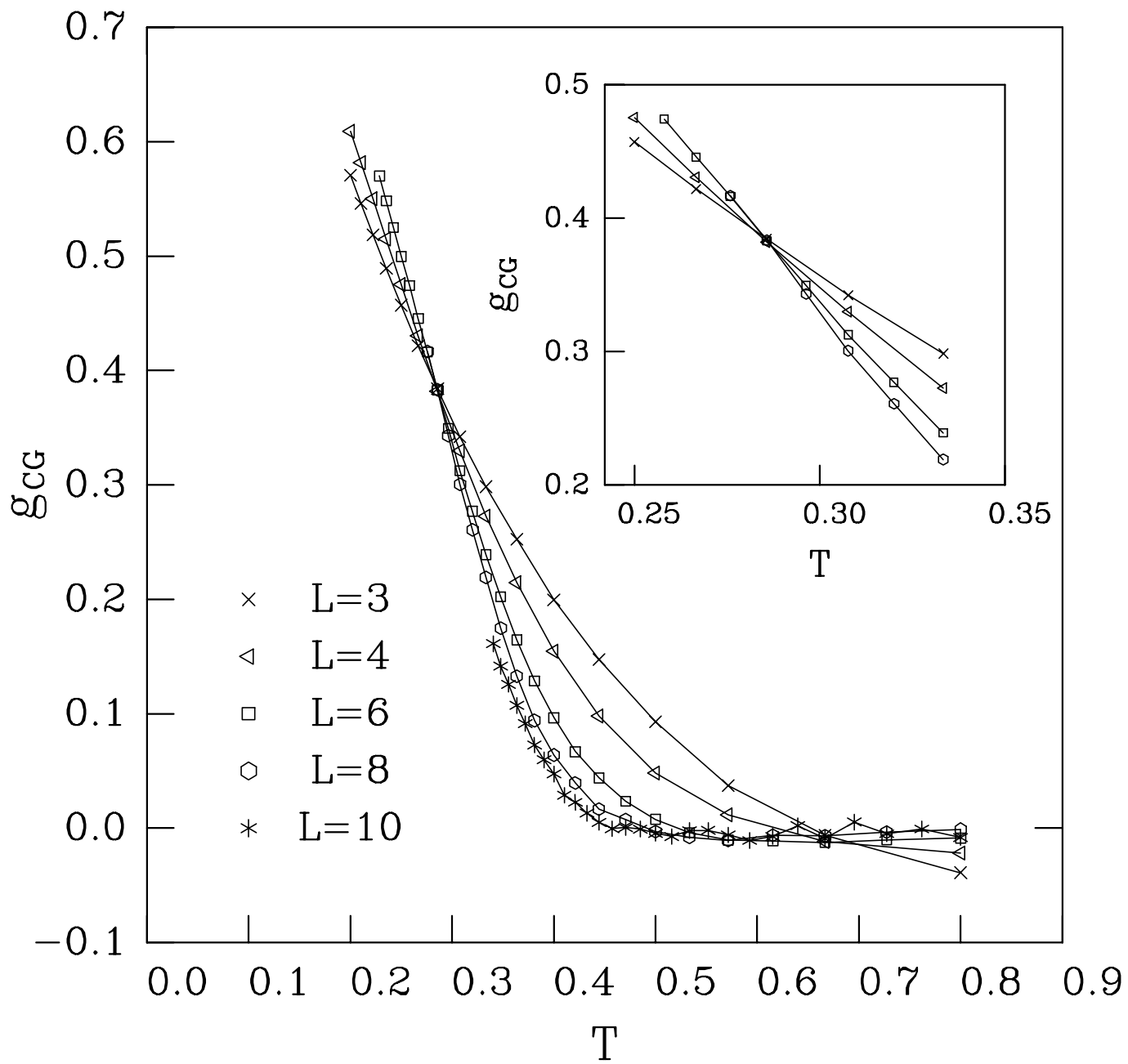
Fig. 16 A phase diagram in the  $T$ - $\tilde{\mathcal{L}}$  plane. Renormalized inductance  $\tilde{\mathcal{L}}$  is defined by Eq.(2.3). The data point at  $\tilde{\mathcal{L}} = 0$  is taken from Ref.17.

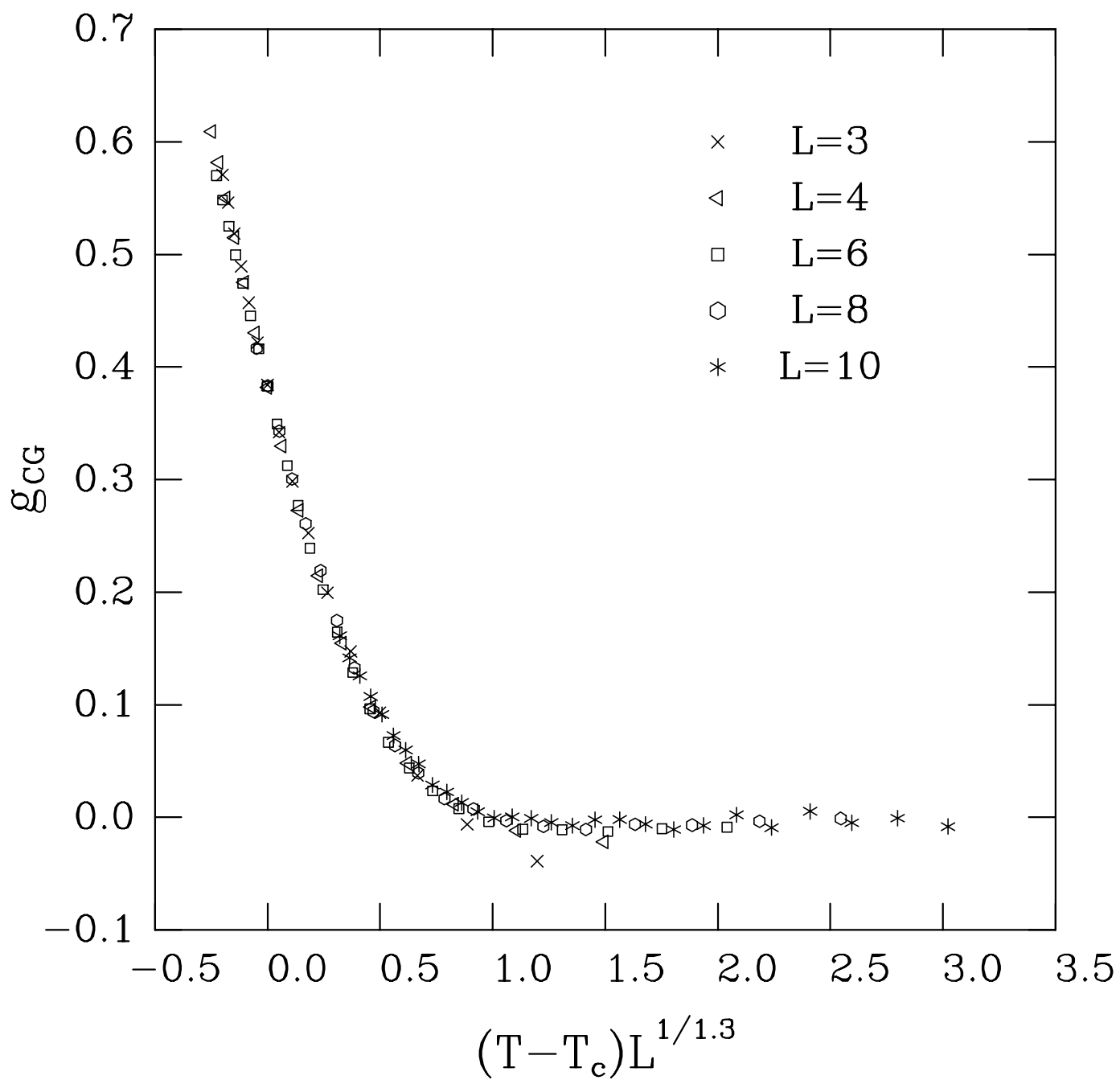
Fig. 17 The temperature and size dependence of the Binder ratio of the flux,  $g_{FG}$ , for (a)  $\tilde{\mathcal{L}} = 4$  and (b)  $\tilde{\mathcal{L}} = 5$ .

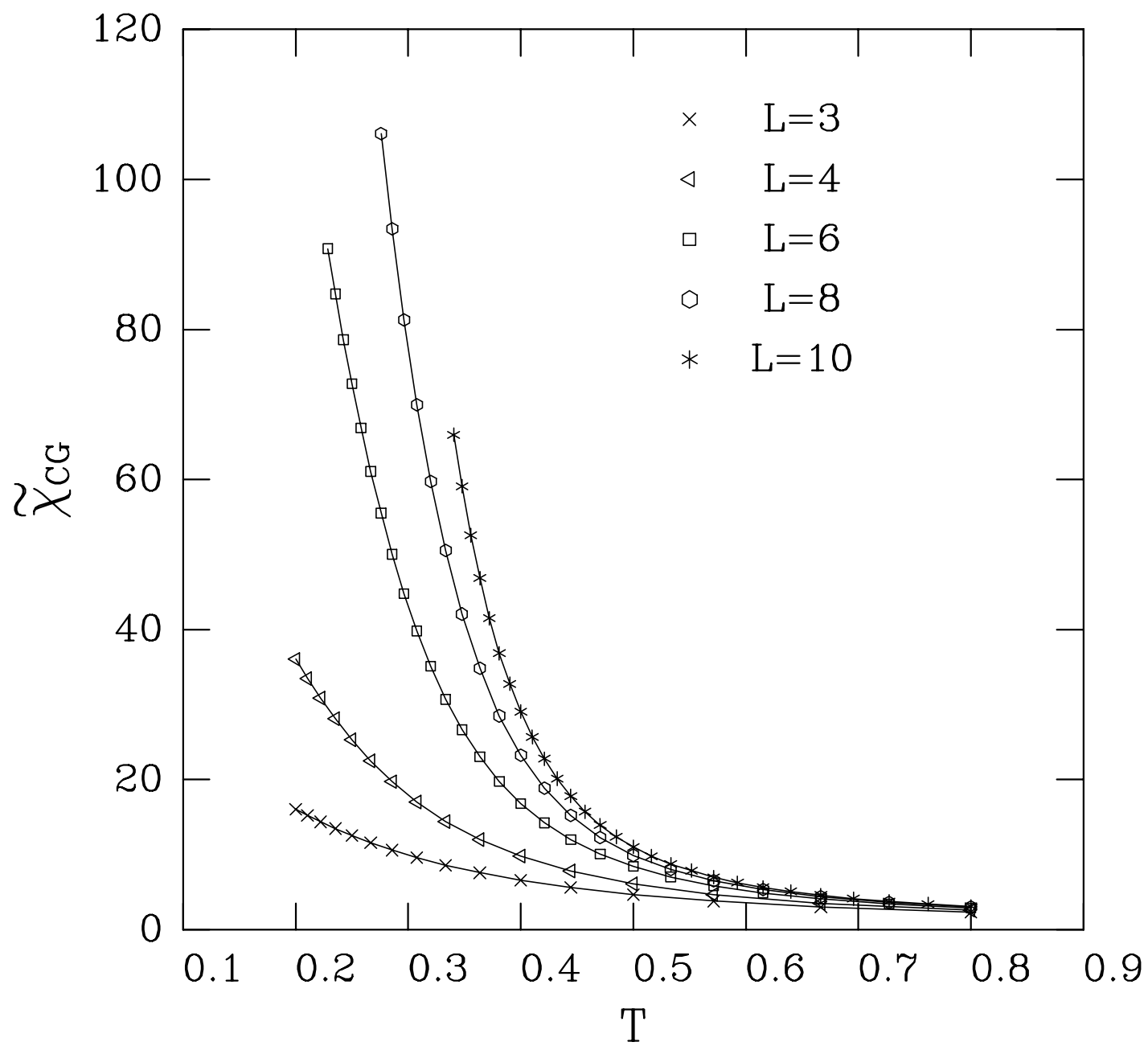
Fig. 18 Two-dimensional segment of the lattice showing thermally-activated integer vortex lines with vorticity  $\pm 1$ , wandering in the background of a frozen pattern of chiralities in the chiral-glass state. Plus (+) and minus (−) chirality can be viewed as half-vortices with vorticity  $\pm 1/2$  sitting at frustrated plaquettes, while unfrustrated plaquettes are frozen into the zero-chirality (0)

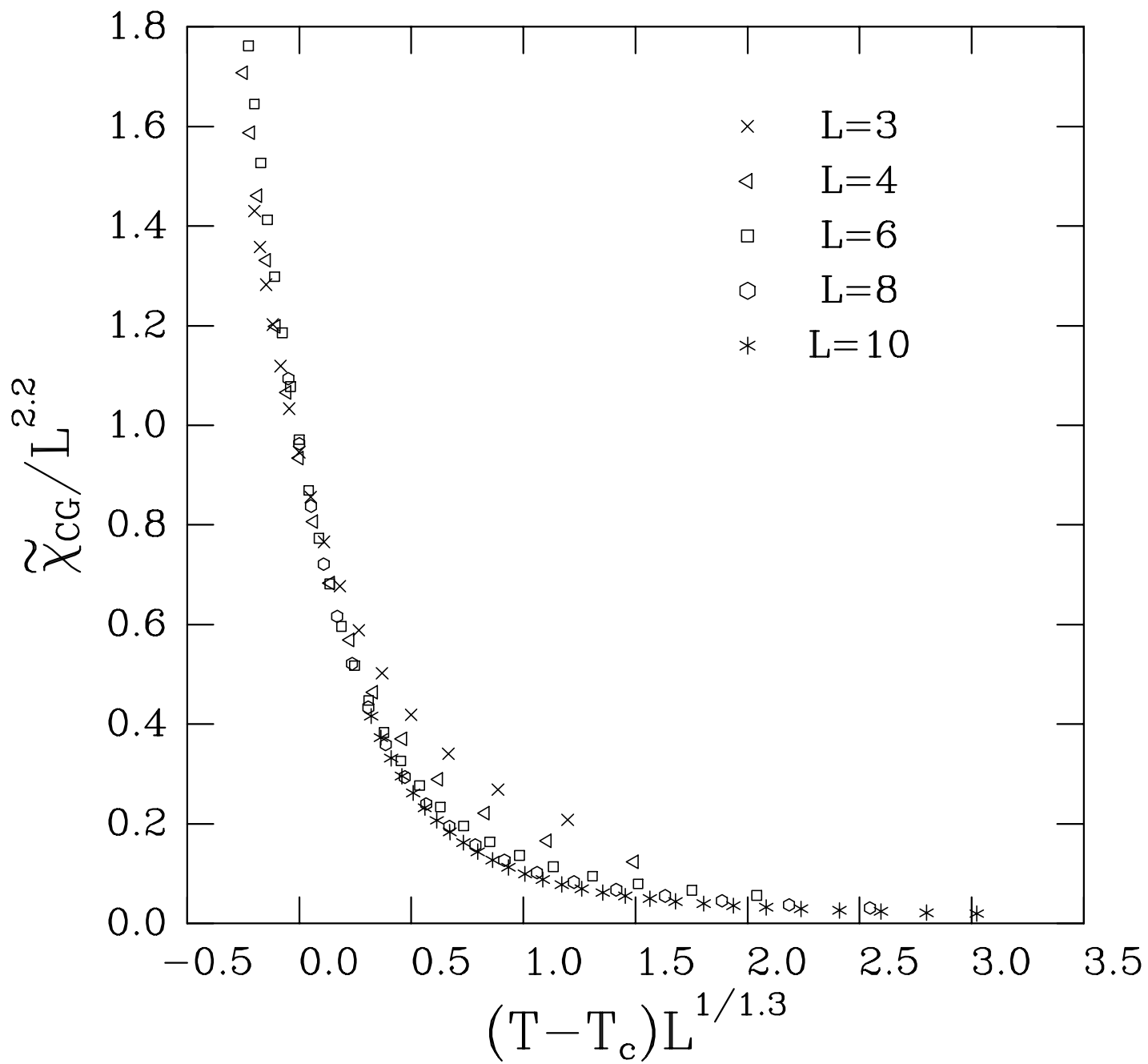
state. If one looks at a given frustrated plaquette frozen into the  $+$  chirality (or vorticity  $+1/2$ ) state, for example, its vorticity occasionally becomes  $+3/2$  or  $-1/2$  when the thermally-activated integer vortex line of either sign,  $+1$  or  $-1$ , passes this plaquette. Still, the long-time average of the vorticity at this plaquette is equal to  $+1/2$ , showing that the free motion of integer vortex lines is compatible with the long-range chiral-glass order.

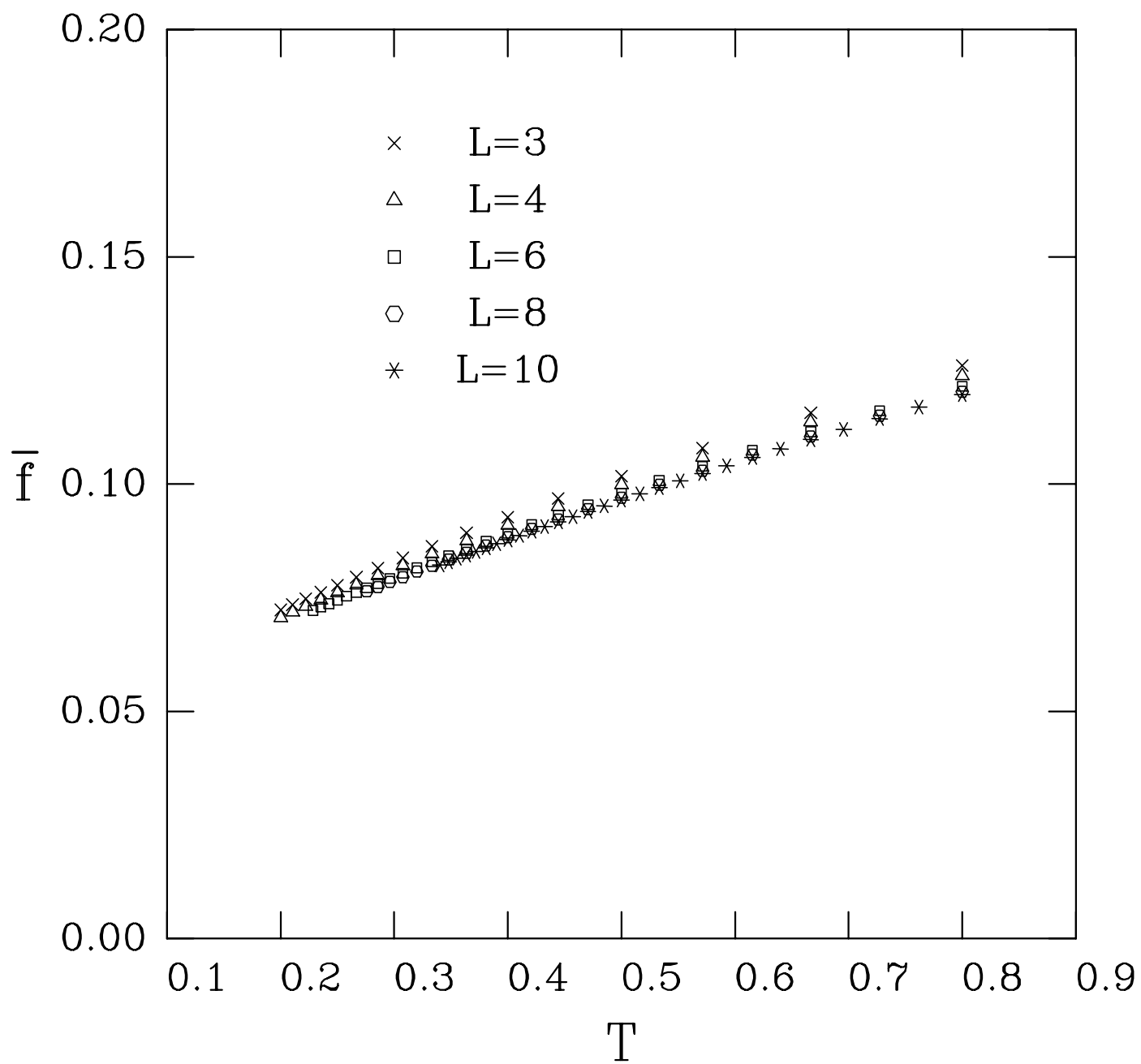


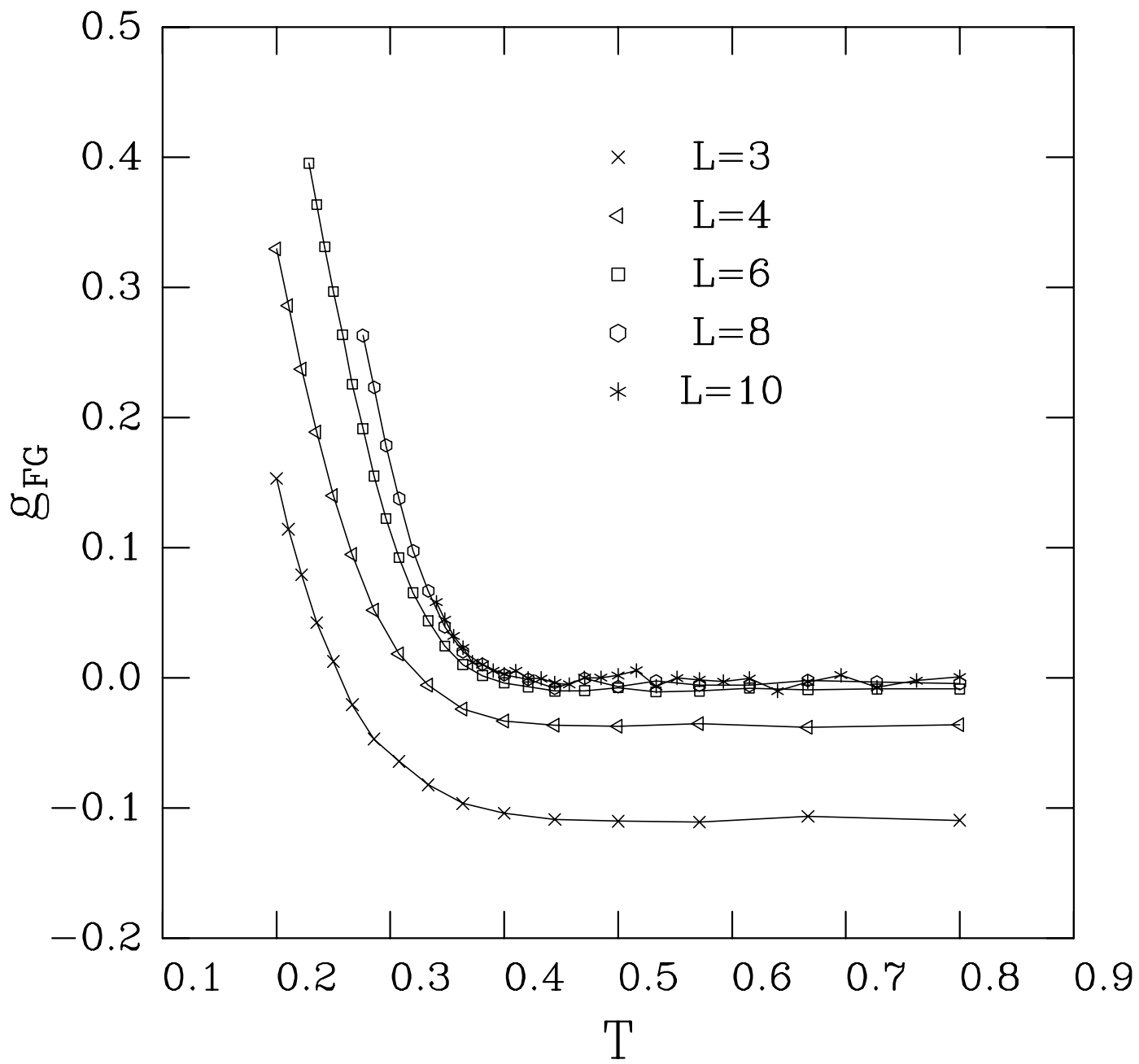


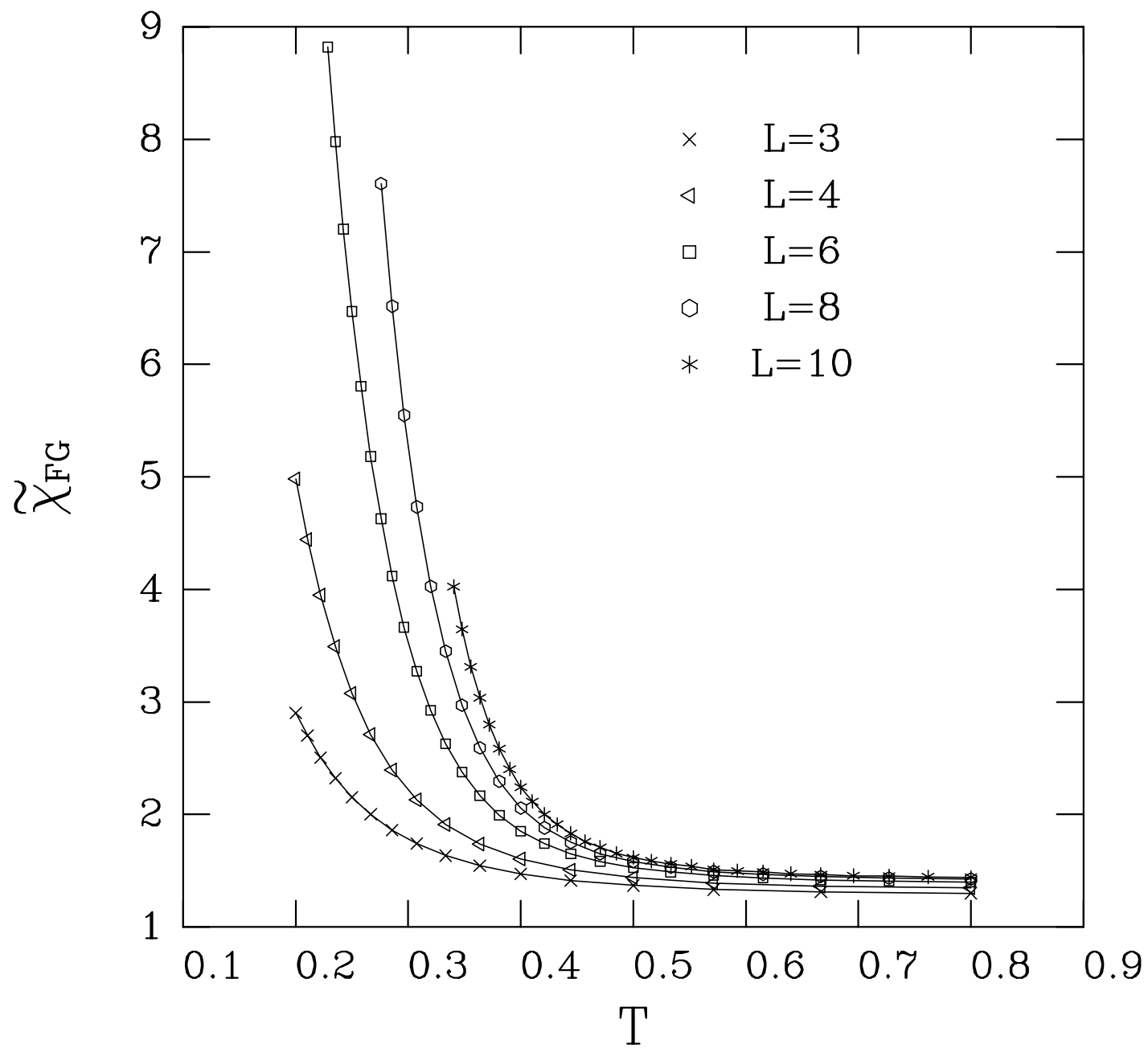


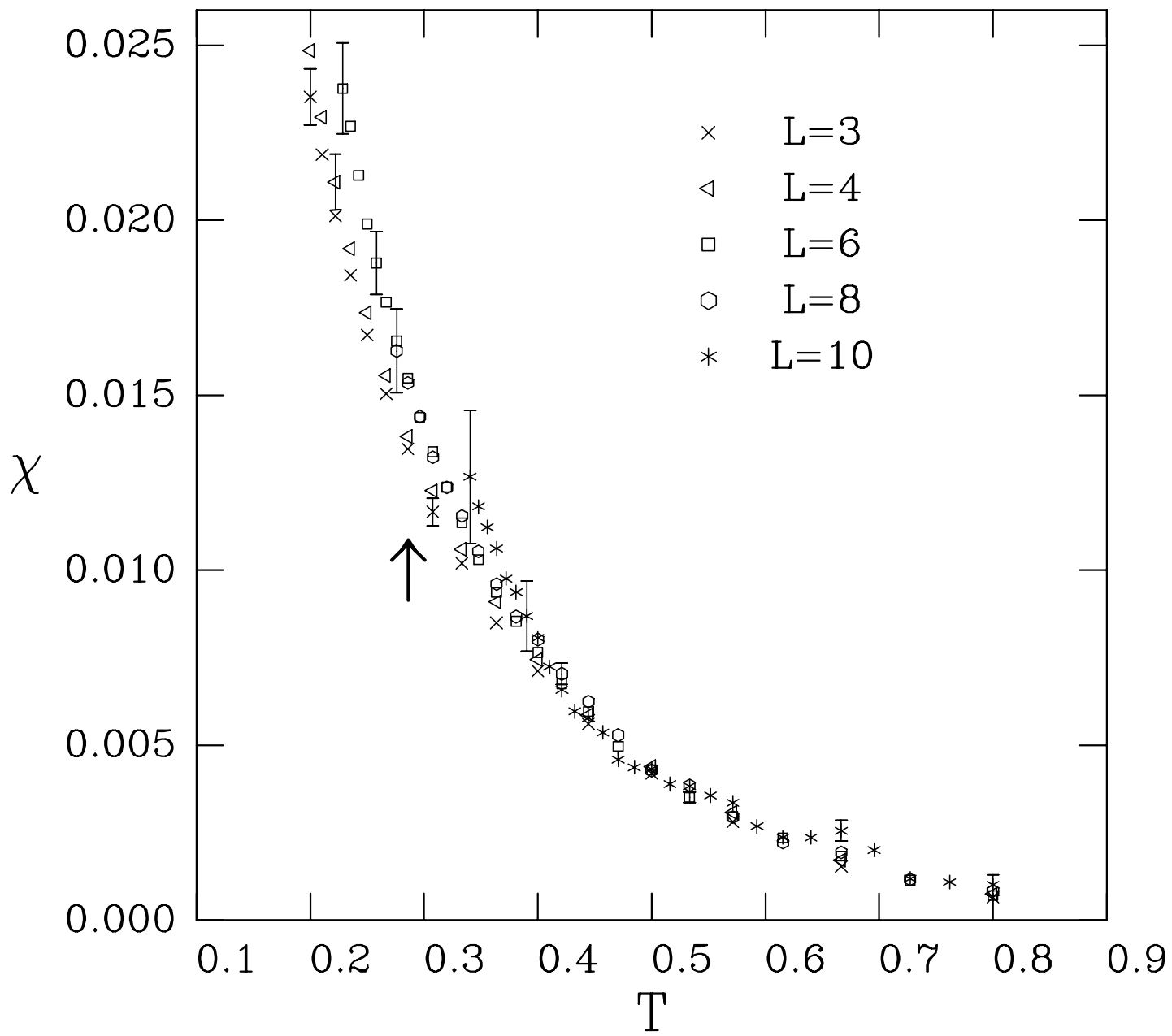


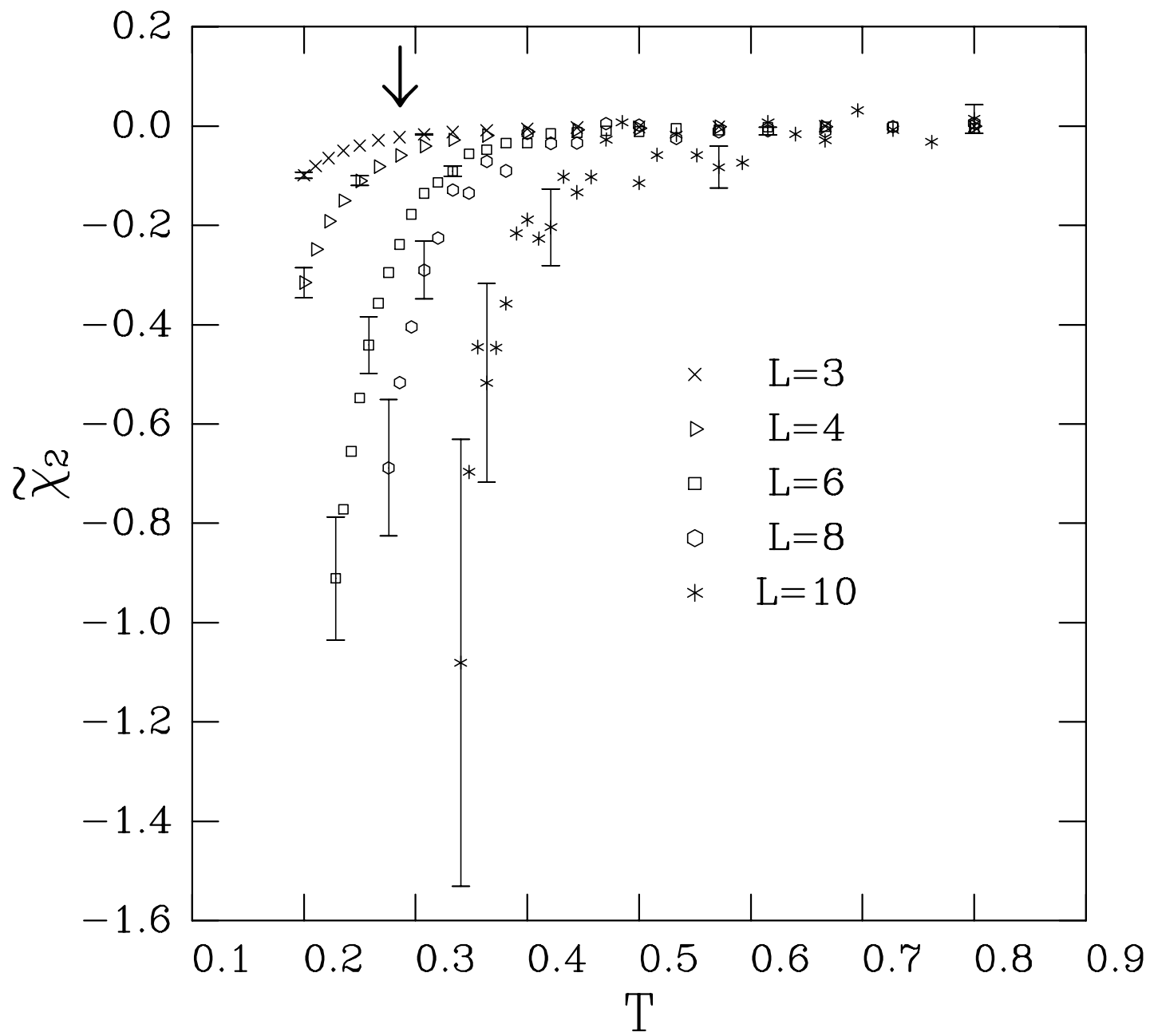


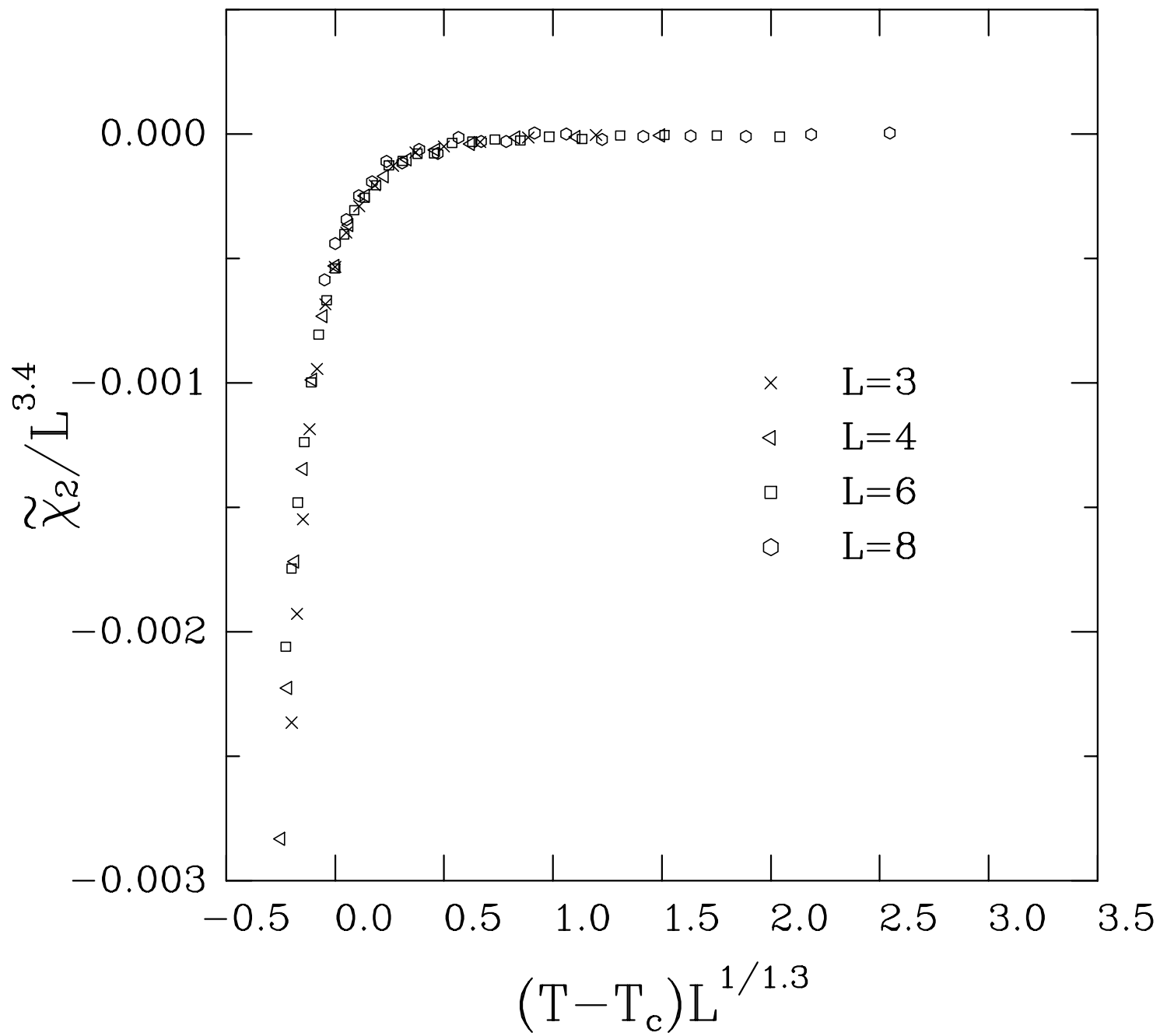


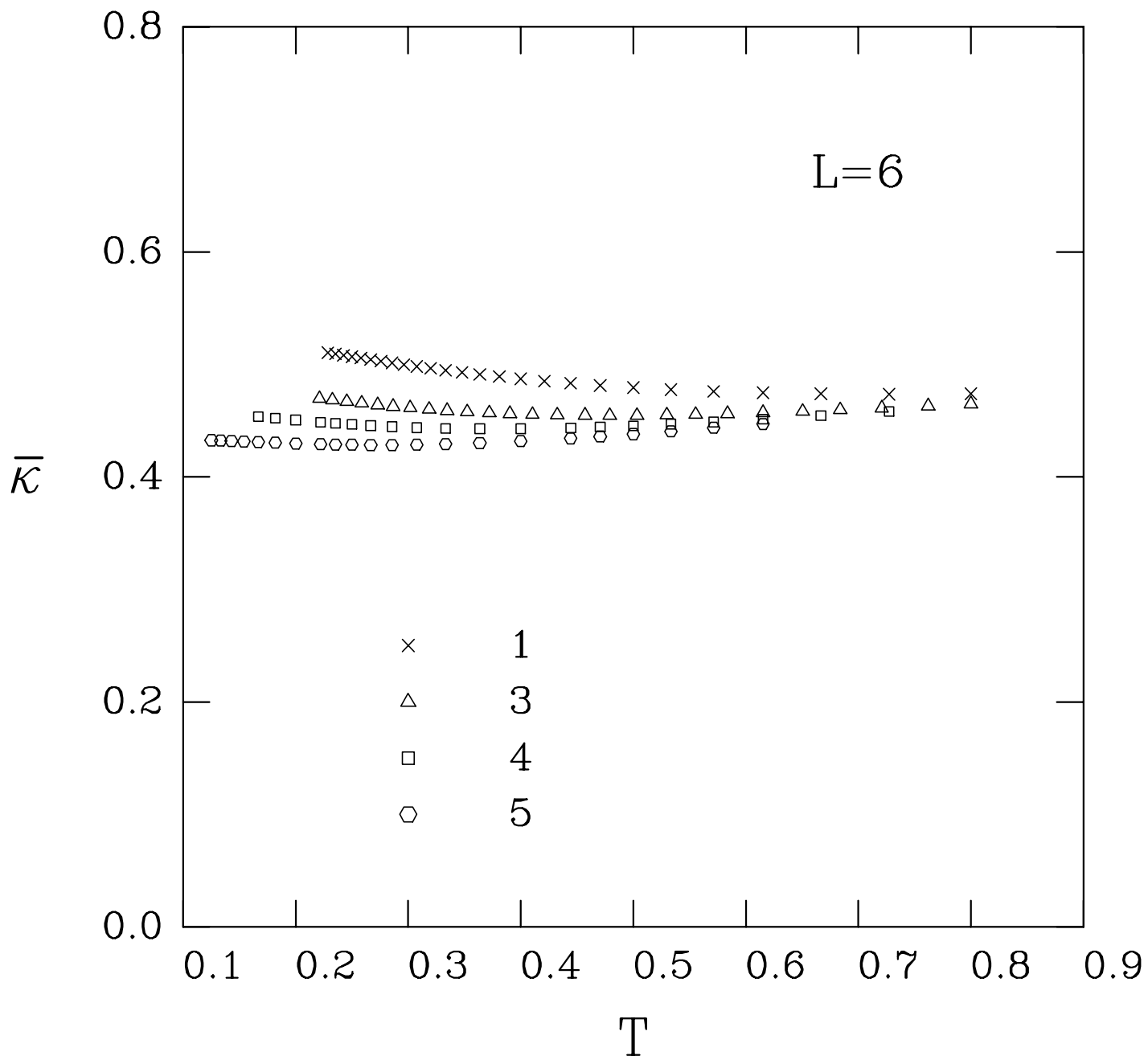


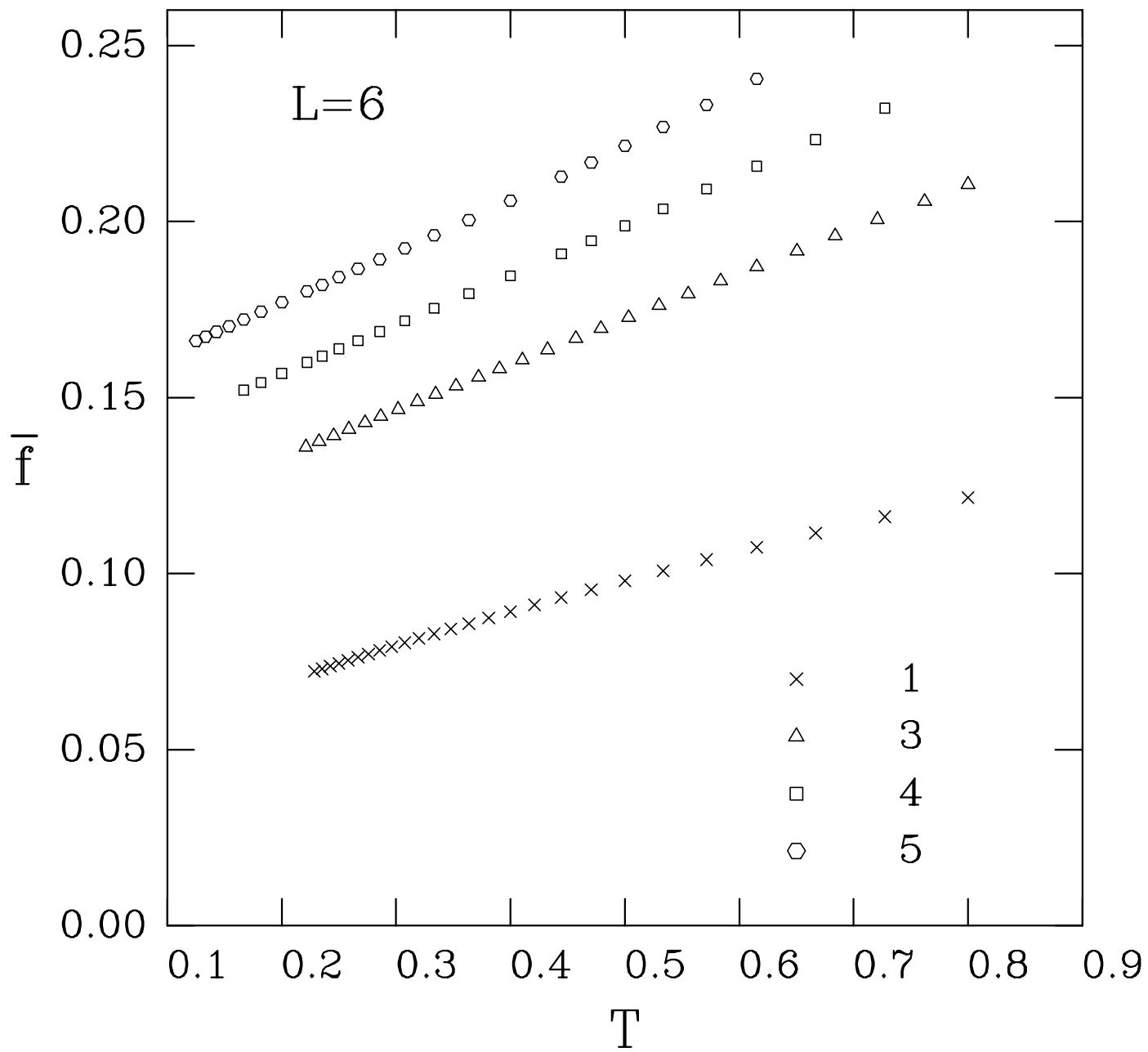


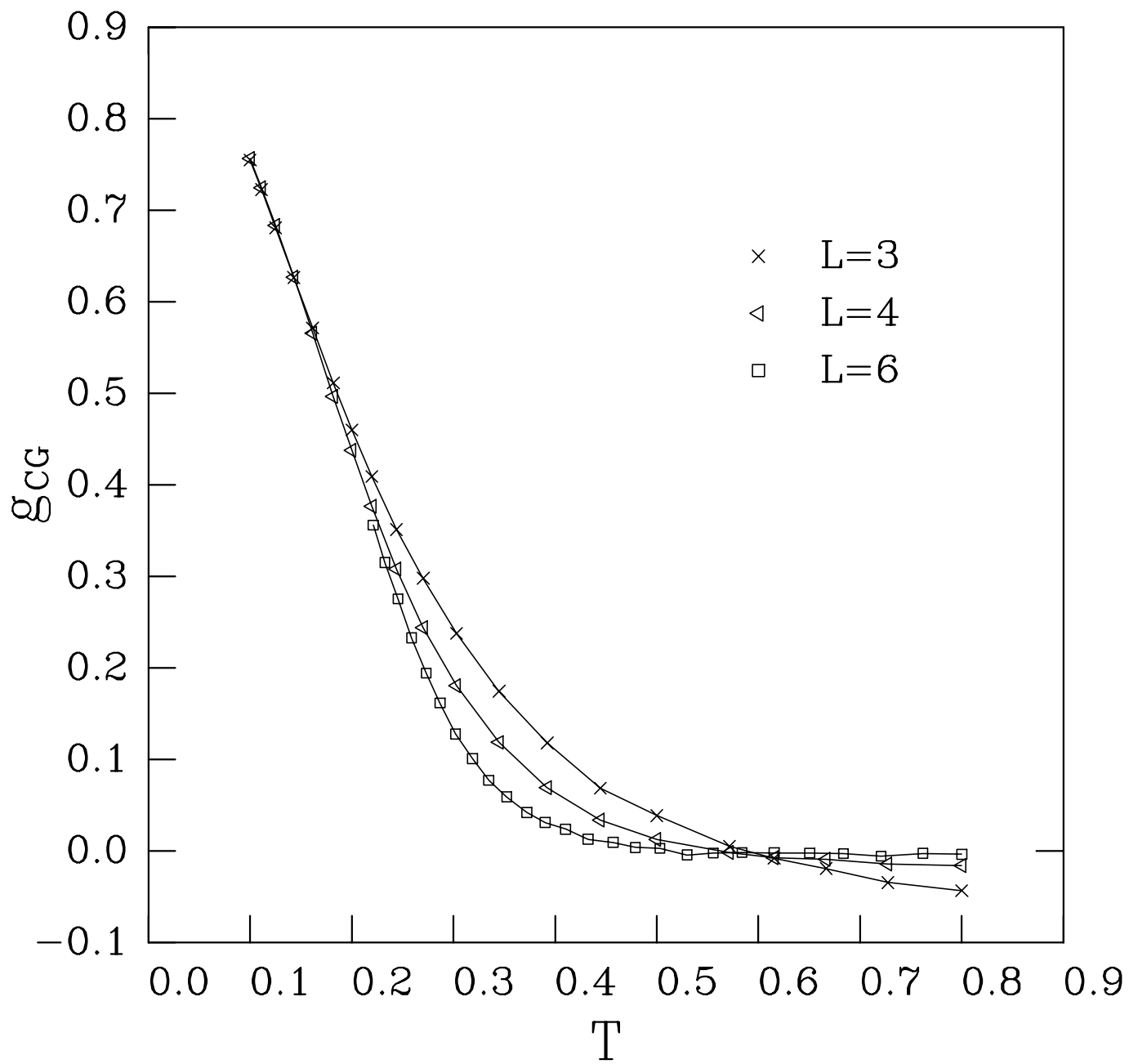


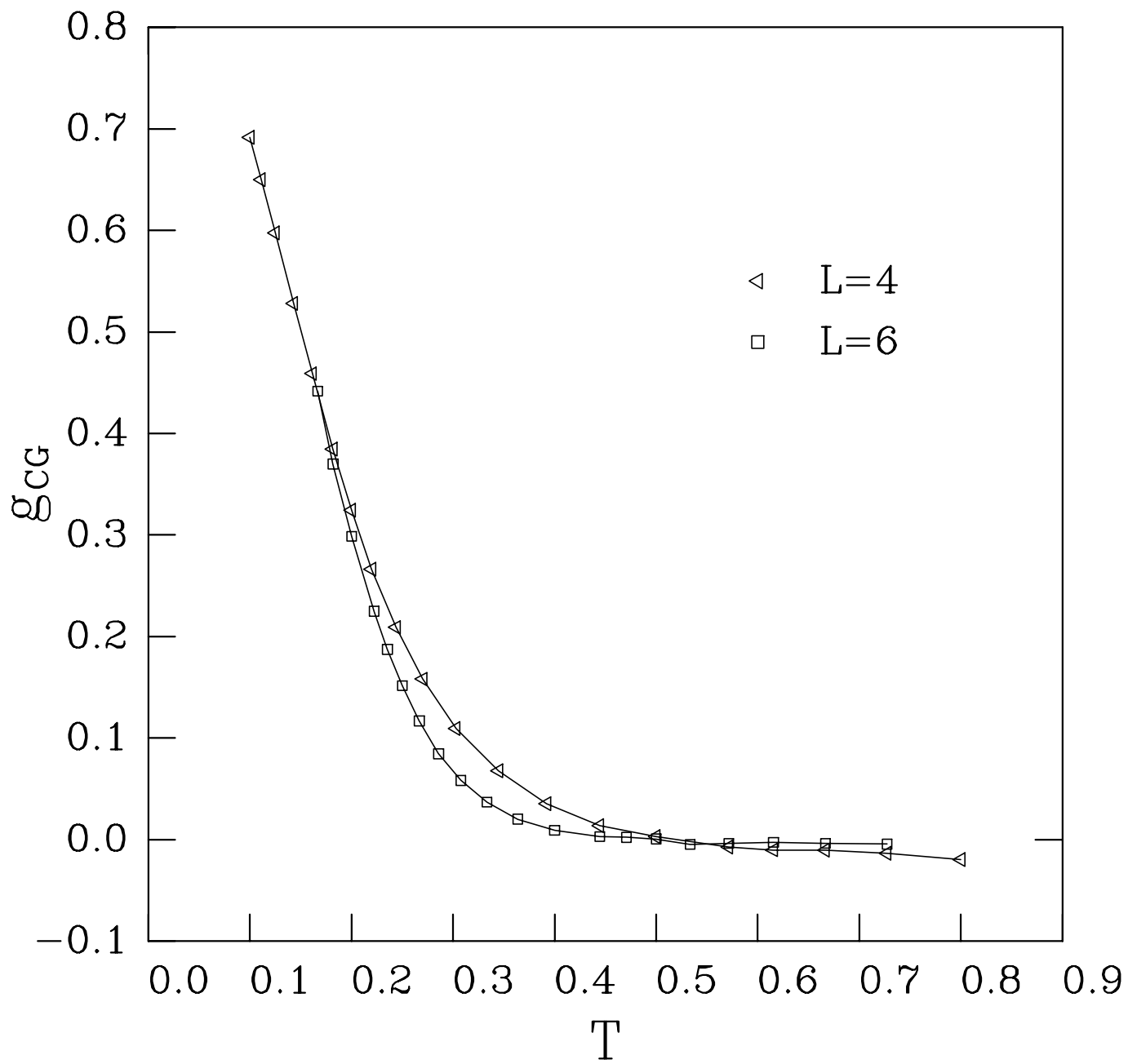


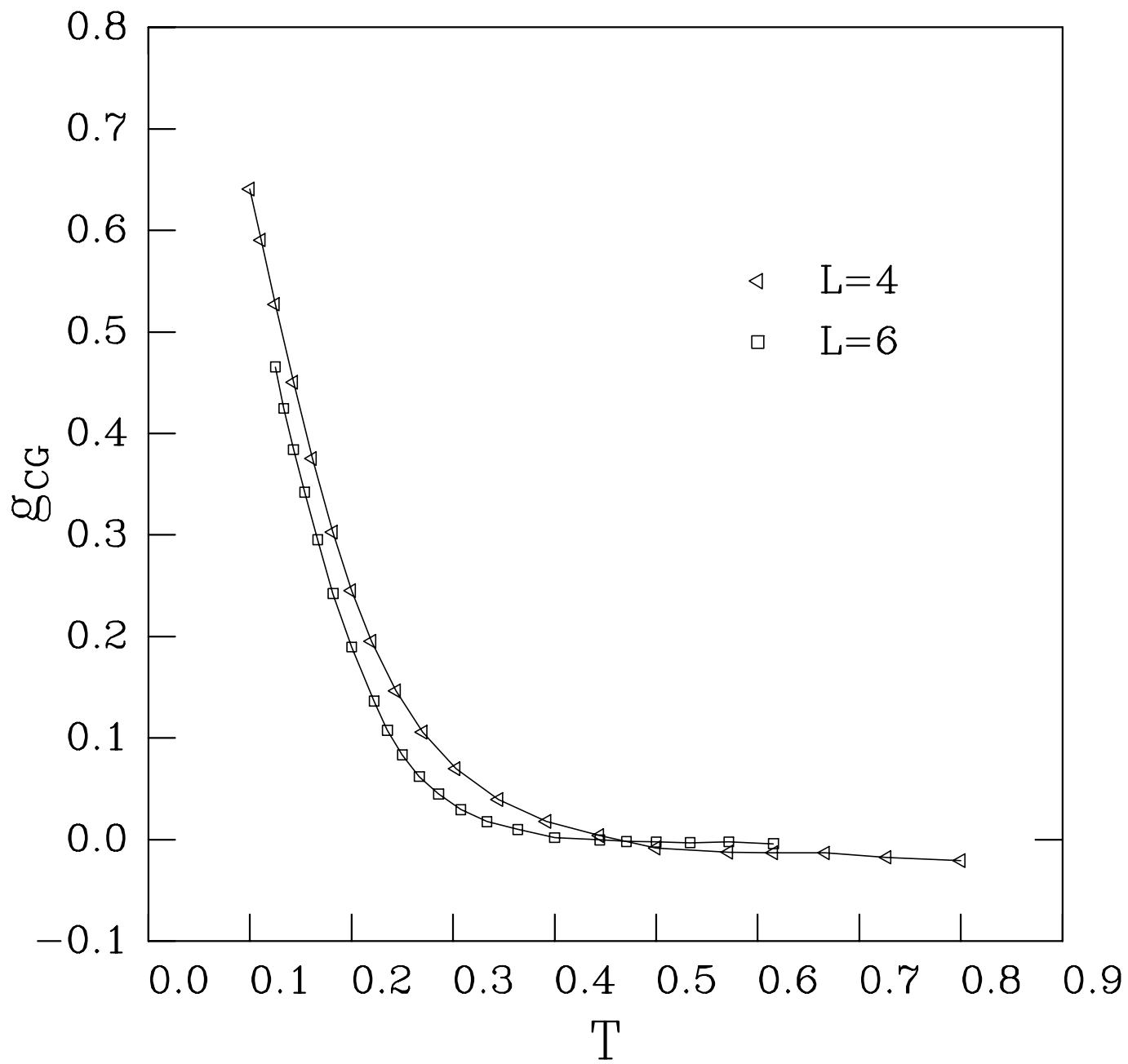


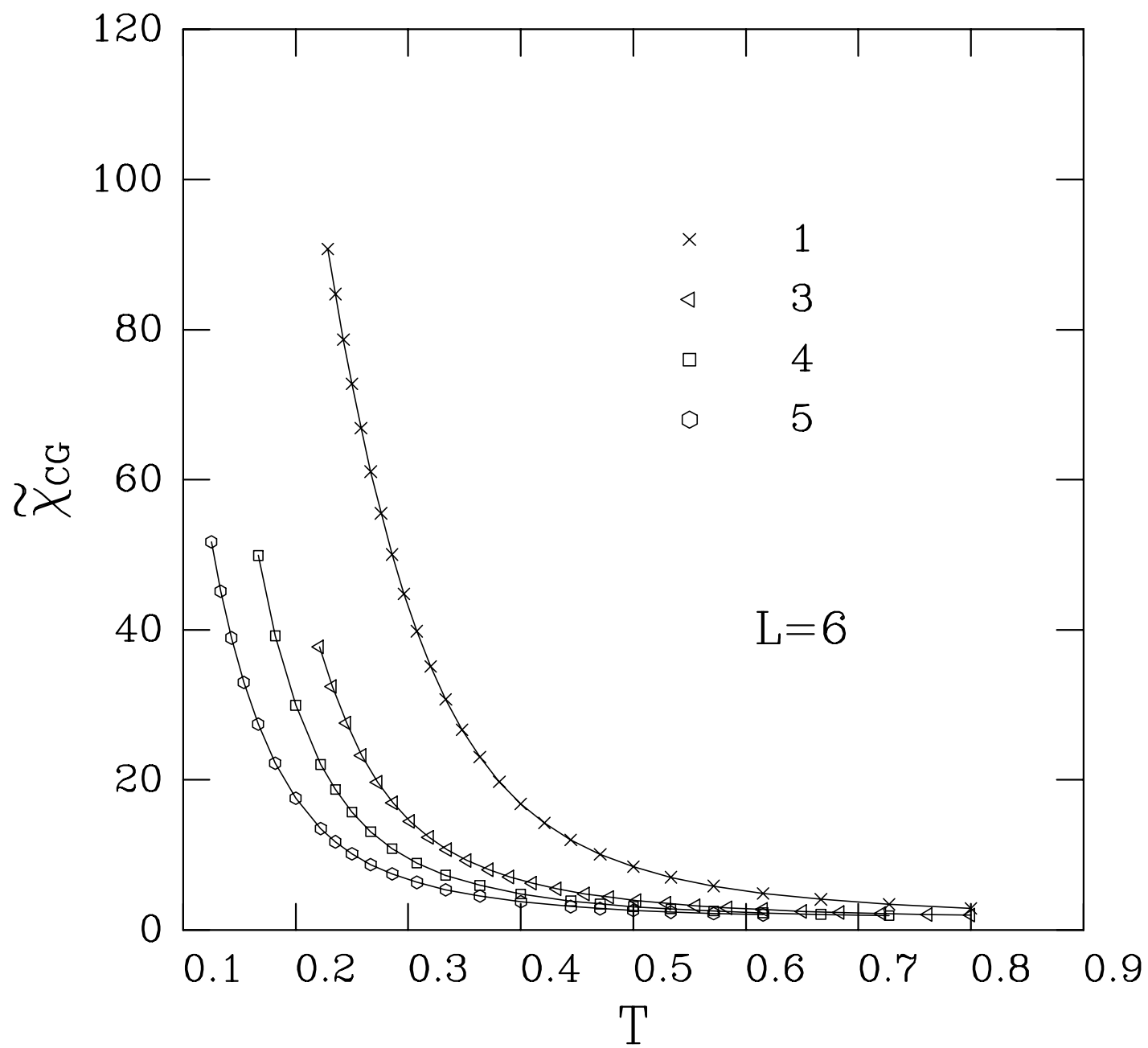


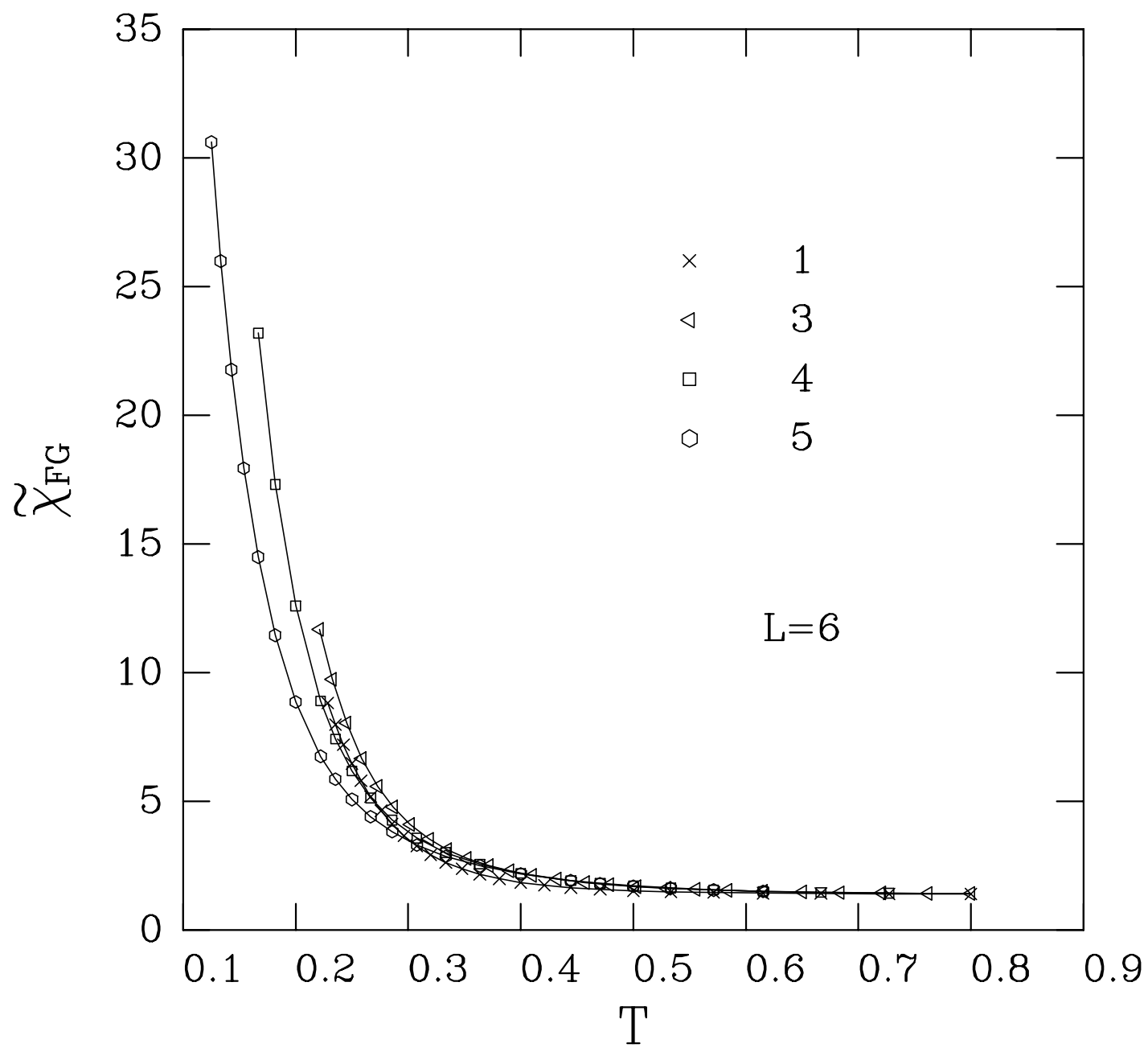


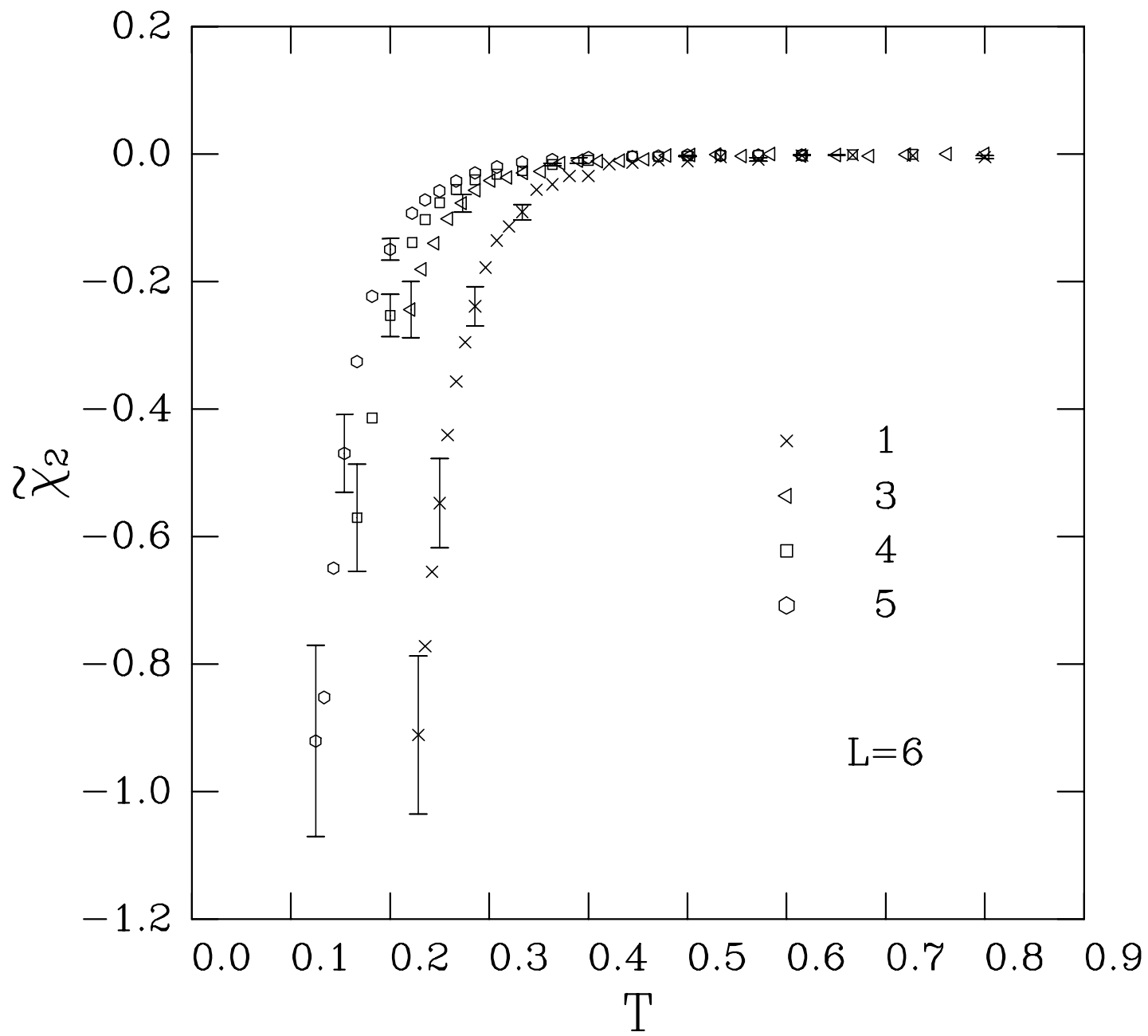


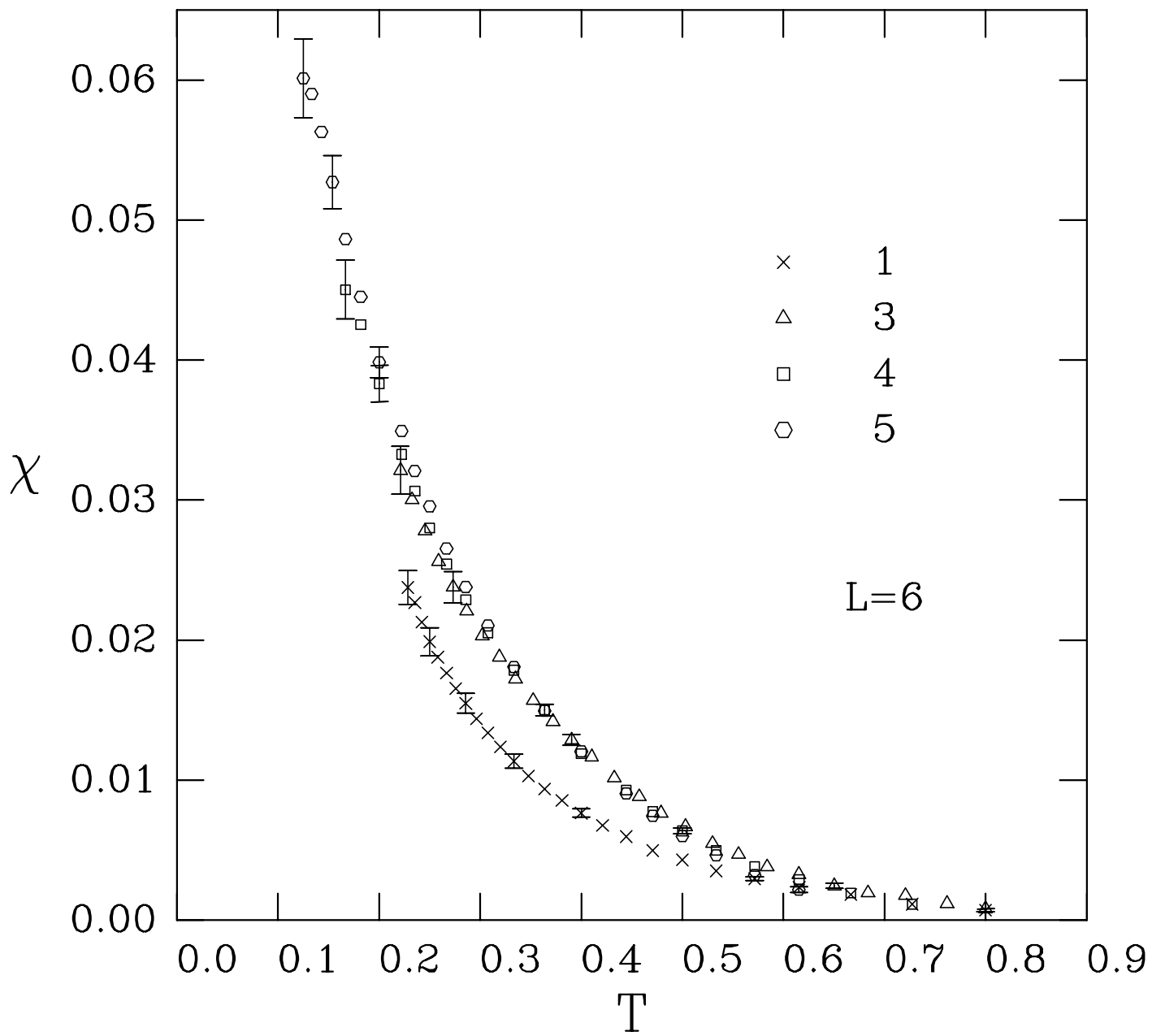


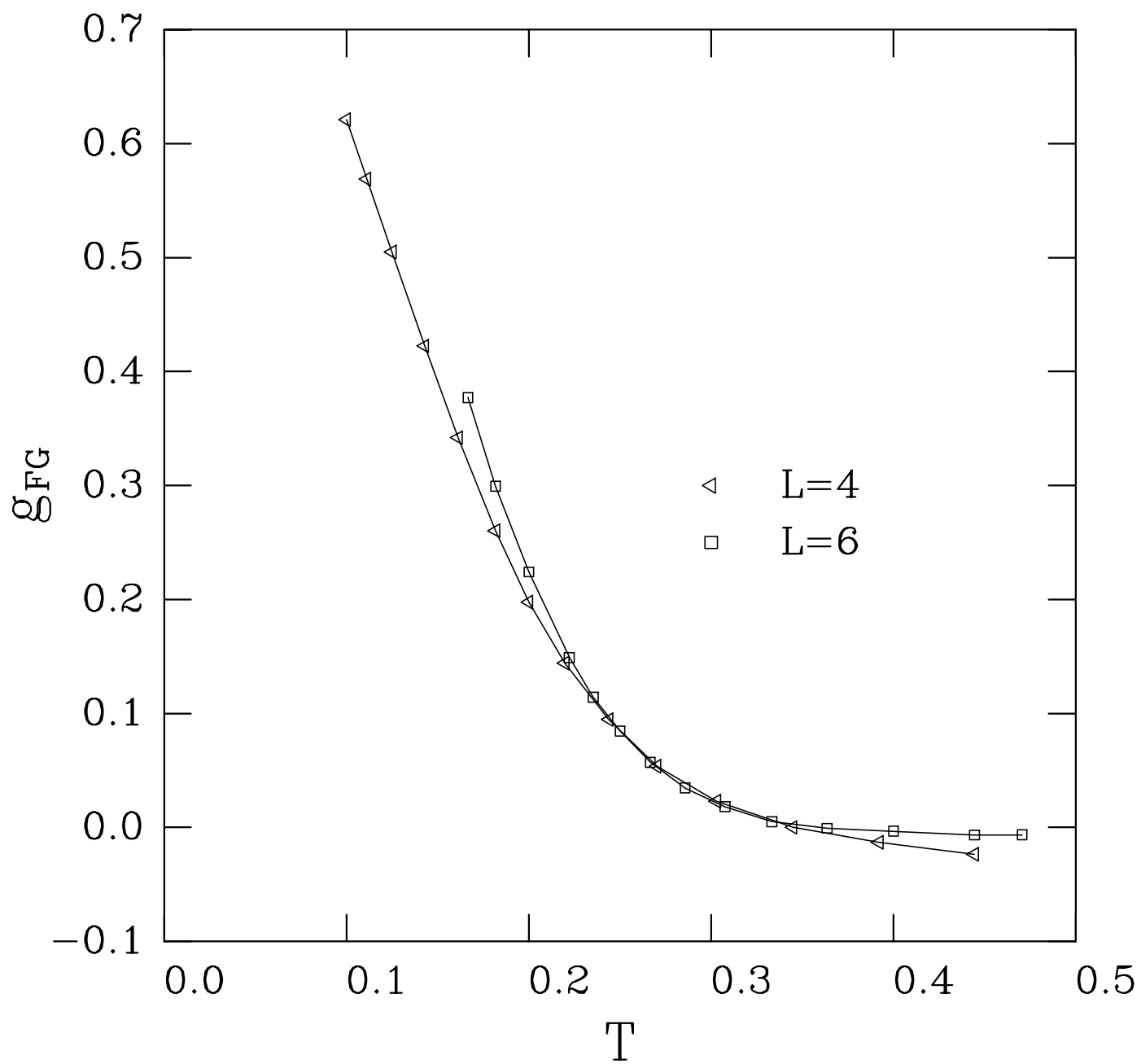


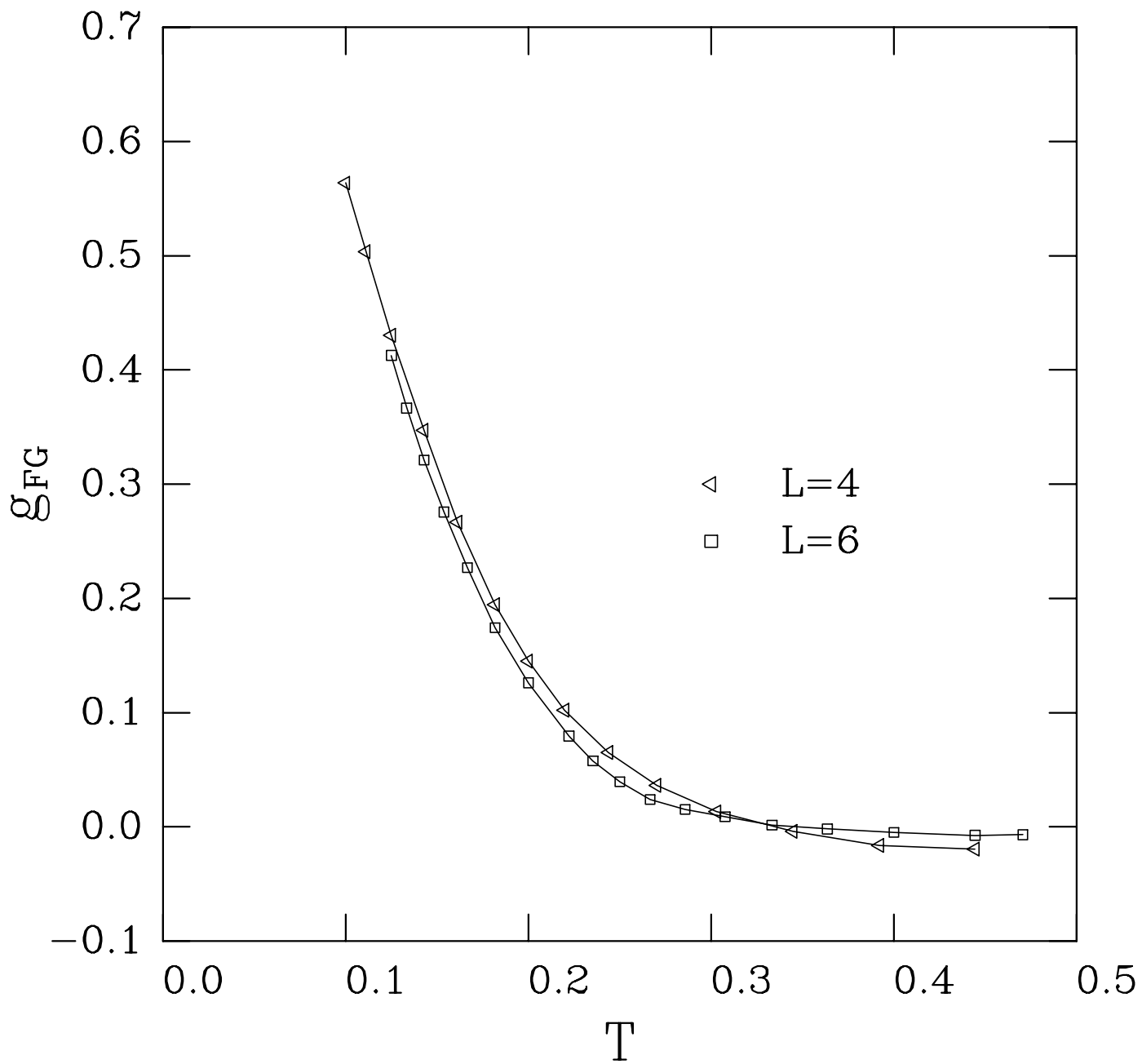












+	-	+	0	0	+	-	-	0	0
0	0	-	+	0	+	-	0	+	+
+	<b>+1</b>	0	0	-	-	+	+	0	0
-	+	+	+	0	0	-	-	0	+
0	0	-	0	0	+	-	+	0	-
0	-	+	+	0	0	0	0	-	+
0	0	0	-	+	-	0	+	0	-
+	+	0	0	0	+	-	<b>-1</b>	+	0
0	0	-	0	+	0	+	-	0	0
+	0	0	-	-	0	0	+	-	+